AFRL-MN-EG-TR-2001-7076

SURFACE LAYER THERMODYNAMICS OF STEEL PENETRATORS AT HIGH AND VERY HIGH SLIDING VELOCITIES

JANUSZ R. KLEPACZKO

UNIVERSITY OF FLORIDA
GRADUATE ENGINEERING AND RESEARCH CENTER
1350 N. POQUITO ROAD
SHALIMAR, FL 32579

JUNE 2001

FINAL REPORT FOR PERIOD 30 APRIL 2001 – 20 JUNE 2001

DISTRIBUTION A: Approved for public release; distribution unlimited.

20030225 087

AIR FORCE RESEARCH LABORATORY, MUNITIONS DIRECTORATE

Air Force Materiel Command ■ United States Air Force ■ Eglin Air Force Base

NOTICE

When Government drawings, specifications, or other data are used for any purpose other than in connection with a definitely Government-related procurement, the United States Government incurs no responsibility or any obligation whatsoever. The fact that the Government may have formulated or in any way supplied the said drawings, specifications, or other data, is not to be regarded by implication, or otherwise in any manner construed, as licensing the holder, or any other person or corporation; or as conveying any rights or permission to manufacture, use, or sell any patented invention that may in any way be related thereto.

This technical report is releasable to the National Technical Information Services (NTIS). At NTIS it will be available to the general public, including foreign nations.

This report has been reviewed for technical content and assessed to be accurate. Due to extenuating circumstances, it is not practical to edit this report for format and it is, therefore, approved "as submitted" by the author.

FOR THE COMMANDER

Paul K Laird

Mr. Paul K. Laird, Technical Director
Ordnance Division

Mr. Kirk E. Herzog, Technical Advisor
Damage Mechanisms Branch

Dr. Mary L. Hughes, Program Manager

Anyone having need of a copy of this report should first contact the Defense Technical Information Center (DTIC) at the address shown below. If you are a registered DTIC User and qualify as a recipient of this document, DTIC can provide you with a copy. If you are a registered DTIC User and do not qualify as a recipient, DTIC can submit a request for release, on your behalf, to the controlling DoD agency for their review and determination. Please do not request copies from the Air Force Research Laboratory, Munitions Directorate. Requests for additional copies should be directed to:

Defense Technical Information Center (DTIC)
8725 John J. Kingman Road, Ste 0944
Ft Belvoir, VA 22060-6218

This report is published in the interest of the scientific and technical information exchange. Publication of this report does not constitute approval or disapproval of the ideas or findings. Do not return copies of this report unless contractual obligations or notice on a specific document requires its return. If you no longer have a need to retain this document, please refer to the Destruction Notice on the cover page for instruction.

If your address has changed, and if you wish to be removed from our mailing list, or if your organization no longer employs the addressee, please notify AFRL/MNMW, 101 W. Eglin Blvd., Ste. 135, Eglin AFB, FL 32542-6810, to help up maintain a current mailing list.

REPORT DOCUMENTATION PAGE

Form Approved
OMB No. 0704-0188

Public reporting burden for this collection of information is estimated to average 1 hour per response, including the time for reviewing instructions, searching existing data sources, gathering and maintaining the data needed, and completing and reviewing the collection of information. Send comments regarding this burden estimate or any other aspect of this collection of information, including suggestions for reducing this burden, to Washington Headquarters Services, Directorate for Information Operations and Reports, 1215 Jefferson Davis Highway, Suite 1204, Arlington, VA 22202-4302, and to the Office of Management and Budget, Paperwork Reduction Project (0704-0188), Washington, DC 20503.

1. AGENCY USE ONLY *(Leave blank)*	2. REPORT DATE	3. REPORT TYPE AND DATES COVERED
	JUNE 2001	FINAL 30 APR 01 - 20 JUN 01

4. TITLE AND SUBTITLE
SURFACE LAYER THERMOMECHANICS OF STEEL PENETRATORS AT HIGH AND VERY HIGH SLIDING VELOCITIES

5. FUNDING NUMBERS
Contract #:
JON:
PE:
PR:
TA:
WU:

6. AUTHOR(S)
JANUSZ R. KLEPACZKO

7. PERFORMING ORGANIZATION NAME(S) AND ADDRESS(ES)
UNIVERSITY OF FLORIDA
GRADUATE ENGINEERING AND RESEARCH CENTER
1350 N. POQUITO ROAD
SHALIMAR, FL 32579
(850) 883-9350

8. PERFORMING ORGANIZATION REPORT NUMBER

9. SPONSORING/MONITORING AGENCY NAME(S) AND ADDRESS(ES)
AIR FORCE RESEARCH LABORATORY, MUNITIONS DIRECTORATE,
DAMAGE MECHANISMS BRANCH (AFRL/MNMW)
101 W. EGLIN BLVD., STE. 135
EGLIN AFB, FL 32542-6810
PROGRAM MANAGER: DR. MARY L. HUGHES (850) 882-7998

10. SPONSORING/MONITORING AGENCY REPORT NUMBER
AFRL-MN-EG-TR-2000-7076

11. SUPPLEMENTARY NOTES

12a. DISTRIBUTION AVAILABILITY STATEMENT
DISTRIBUTION A: Approved for public release; distribution unlimited.

12b. DISTRIBUTION CODE

13. ABSTRACT *(Maximum 200 words)*

One of the most difficult problems in the mechanics of kinetic energy projectiles penetrating geological or cementitious target materials is a proper understanding of the frictional properties between the projectile surface and the target. The model developed in this study is limited to a simple definition of the state of the projectile surface as a set of uniformly distributed micro-asperities with the same active height, h = 20 microns, which are subject to fast adiabatic shearing. Although the heat conduction equation has not been solved numerically in this study, a useful approximation of the evolution of temperature in the bulk material was applied. This approximation permitted finding the closed form solution for the homologous bulk temperature, at different sliding conditions. Because evolution of the bulk temperature could be estimated, it also permitted finding the evolution of the coefficient of friction as a function of the sliding velocity. For every definition of the coefficient of friction a substantial decrease of the resistance to sliding at increasing velocities has been found. An open question remains as to the role of the hydrostatic pressure. For example, the experimental data suggest that at constant velocity the coefficient of friction will diminish as a function of pressure as predicted by Eq. (51). Thus, an advantage of the model presented here is that hydrostatic pressure can be taken into consideration in a correct way. Albeit implementation of the friction model in the form of Eq. (51) into numerical codes is rather too early, preliminary trials should be recommended.

14. SUBJECT TERMS
Thermomechanics; Penetrators; Friction; Wear; High Velocity; Penetration; Geological Targets; Concrete; Projectiles; Coefficient of Friction; Thermodynamics; Asperities

15. NUMBER OF PAGES
73

16. PRICE CODE

17. SECURITY CLASSIFICATION OF REPORT	18. SECURITY CLASSIFICATION OF THIS PAGE	19. SECURITY CLASSIFICATION OF ABSTRACT	20. LIMITATION OF ABSTRACT
UNCLASSIFIED	UNCLASSIFIED	UNCLASSIFIED	UL

SURFACE LAYER THERMOMECHANICS OF STEEL PENETRATORS AT HIGH AND VERY HIGH SLIDING VELOCITIES

PREPARED BY

JANUSZ R. KLEPACZKO*

University of Florida

Graduate Engineering & Research Center

1350 N. Poquito Road

SHALIMAR FL 32579

April 2001

*Visiting Professor

Laboratory of Physics and Mechanics of Materials

Metz University

Ile du Saulcy, F-57045 Metz, France

Abstract

One of the most difficult problems in the mechanics of KE projectiles penetrating geological or cementitious target materials is a proper understanding of the frictional properties between the projectile surface and the target. The model developed in this study is limited to a simple definition of the state of the projectile surface as a set of uniformly distributed micro-asperities with the same active height h = 20 μm, which are subject to fast adiabatic shearing. Although the heat conduction equation has not been solved numerically in this study, a useful approximation of the evolution of temperature in the bulk material was applied. This approximation permitted finding the closed form solution for Θ_b, the homologous bulk temperature, at different sliding conditions. Because evolution of the bulk temperature could be estimated, it also permitted finding the evolution of the coefficient of friction as a function of the sliding velocity. For every definition of the coefficient of friction a substantial decrease of the resistance to sliding at increasing velocities has been found. An open question remains as to the role of the hydrostatic pressure. For example, the experimental data suggests that at constant velocity the coefficient of friction will diminish as a function of pressure as predicted by Eq.(51). Thus, an advantage of the model presented here is that the hydrostatic pressure can be taken into consideration in a correct way. Albeit implementation of the friction model in the form of Eq.(51) into numerical codes is rather too early, preliminary trials should be recommended.

List of symbols and abbreviations

Symbol	Page	Definition
F_t	5	tangential force
F_n	5	normal force
μ	5	coefficient of friction
ASB	5	adiabatic shear banding
HAZ	7	heat affected zone
h_n	7	asperities with randomly distributed heights
N	7	total number of asperities
S	7	surface area
N	7	density of microasperities
N_a	7	uniformly distributed array of active microasperities
Λ	8	mean dimension of elementary cell
f_a	8	fractional area of active microasperities
S_o	8	domain of surface without contact
S_a	8	active surface
S_b	8	passive surface (Coulomb friction)
N_0	8	number of asperities with no contact
N_a	8	number of active asperities
N_b	8	number of passive asperities
f_{n0}	8	fraction of asperities without contact
f_{na}	8	fraction of active asperities
f_{nb}	8	fraction of passive asperities
a,b,c	8	side dimensions of active, passive, and no contact asperities, respectively
$\Lambda_a, \Lambda_b, \Lambda_c$	8	mean distances between microasperities
n_a, n_b, n_c	9	densities of respective asperities
p	9	pressure
M	9	constant: propensity of active asperities to grow in number

Symbol	Page	Definition
B	9	constant: probability of interaction between neighboring microasperities
$\overline{F}_x$	10	mean tangential force
$\overline{F}_y$	10	mean normal force
τ_a, τ_b	11	shear stresses on particular micro-asperities
σ_a, σ_b	11	normal stresses on particular microasperities
τ_{eff}	11	effective shear stress
f_{a0}	12	fractional area of active microasperities at initial condition
τ_y	12	yield stress in shear
$\dot{\Gamma}$	13	shear strain rate
$\hat{\tau}_0$	14	shear stress mechanical threshold at 0 K
$\dot{\Gamma}_{c0}$	14	critical shear strain rate required to activate dislocation motion without assistance of thermal vibration, i.e. at 0 K
l_m	14	length of a mobile dislocation
B	14	viscous drag
$\overline{v}$	14	mean dislocation velocity
b	14	Burgers vector
ρ_m	14	mobile dislocation density
η	15	pseudo-viscosity
C_2	15	speed of elastic shear wave
G	15	shear modulus
ρ_0	15	mass density
$\dot{\Gamma}_{crit}$	15	critical strain rate in shear
η_0	15	pseudo-viscosity at 0 K
θ	16	homologous temperature
T, T_m	16	absolute temperature and melting temperature
G_0	16	shear modulus at $\theta = 0$
A, B	16	constants used in eqn (36)
C_v	17	specific heat at constant volume
λ	17	heat conductivity
t	17	time

Symbol	Page	Definition
β	17	fraction of the plastic work converted into heat
Γ	17	shear strain
Γ_c	18	failure shear strain
Γ_f	18	critical shear strain
t_f	18	time interval to failure
t_c	19	time to failure
t_i	19	interval of time required to heat an asperity to specific temperature
t_p	20	time of penetration
L_p	20	penetrator length
H	20	characteristic thermal diffusion depth during penetration
v_c	20	frequency of asperity cutting
α	20	characteristic constant
T_b	21	bulk temperature in K
Θ_b	21	homologous bulk temperature
R_μ	23	ratio of coefficients of friction
μ_0	26	quasi-static coefficient of friction at V = 1 m/s

1. Introduction

The most difficult problem in the penetration mechanics of steel projectiles into a concrete target is a proper understanding of frictional properties between the projectile surface and the perforated medium. Since velocities of penetration are very high, of the order of 1,500 m/s, and the pressure on the projectile surface is very high as well, this unique combination of parameters makes the problem difficult. The initial kinetic energy of a projectile might be very high, since it increases proportionally with the second power of velocity. Thus, there is no linear relation between those two quantities. The main factor that governs the penetration distance is the force due to the target resistance superimposed on the friction conditions present between the projectile and the target. Many physical processes may occur during a high-speed penetration; for example, erosion of the projectile surface accompanied by high temperatures and possible phase transformation, on or near the steel surface, transportation of the melted material onto the shank, injection of the melted material into the target medium and chemical reactions on the surface like fast oxidation. Those physical processes which are involved in penetration mechanics cause the estimation of a "mean" coefficient of friction in the Coulomb sense, that is $F_t = \mu F_n$ (where F_t, F_n and μ are respectively the tangential force, the normal force and the coefficient of friction) to become extremely difficult. It can be shown that the coefficient of friction defined in such a manner is *not a constant* but depends on many factors like sliding velocity, normal pressure, composition of penetrated material (aggregate size and paste), and on the yield stress, rate of thermal softening, thermal conductivity, specific heat and melting temperature of the projectile material. In conclusion, a more detailed study of friction conditions on the projectile interface is of great importance to derive alternative friction laws based on the principles of physics. Recent studies on abrasion and penetration (mostly numerical) [1,2,3], clearly indicate the prudent direction of future efforts.

During the last few decades substantial progress has been witnessed in understanding temperature-coupled processes of plastic deformation. One such process is Adiabatic Shear Banding (ASB). Many publications have appeared concerning this topic, including monographs – see, for example Reference [4], along with the information recorded in References [5-10]. The mechanism of ASB is relatively simple – the work of plastic deformation, converted largely into heat, softens the material, leading to instability and

localization of plastic deformation. The process is repeated in a loop and the final result is a very narrow band of severe plastic deformation ranging in width from 5 to 100 micrometers. As it has been shown in Reference [10] many physical factors influence triggering and evolution of the ASB. A complicated interplay between strain hardening, thermal softening, strain rate sensitivity, thermal conductivity and sometime local inertia occurs in an ASB. In some materials, particularly in steels and titanium alloys, a phase-like transformation can take place within a narrow zone of the highest temperature. The ASBs, with or without phase transformation, often act as sites of Mode II fracture initiation.

It has also been shown that formation of ASBs depends on the initial and boundary conditions [10,11]; in particular, the velocity imposed on a deforming body is one of the main factors influencing the evolution of an ASB. If the imposed velocity is high, on the order of 100 m/s, the Critical Impact Velocity in shear is reached [12,13], and a localization of plastic deformation will occur on the surface where that velocity is imposed. Importance of the roles ASBs play in diverse processes like rolling, machining, drawing, impact on structures, ballistic impact and fragmentation of metals and alloys is obvious. One recent illustration is an analysis of the coefficient of friction in high-speed machining [14]. Additionally, it has been shown that application of the ASB concept to analysis of friction at velocities from 1 m/s to 100 m/s leads to reasonable agreement with experimental data [15,16]. In these studies, the adiabatic shear banding approach to the process of surface sliding is extended to high and very high velocities, similar to those encountered in penetration mechanics.

2. Fundamental assumptions and the surface algebra

Since every surface has a certain level of roughness, during sliding the tops of the highest asperities will be loaded by a high shear stress. If the sliding velocity is sufficiently high the tops of the highest asperities will be cut by adiabatic shear banding. The debris of the tops is the source of the surface erosion. Since the localization process of plastic deformation in ASB produces high temperature, the active asperities will become the "hot points" and the heat generated will be transmitted into the bulk of the material. Because the process of adiabatic cutting will be repeated with a high frequency at random places on the surface, the bulk material will be constantly heated until the sliding is ended. This mechanism produces very

high temperature gradients close the surface of the bulk material, developing a Heat Affected Zone (HAZ) not necessarily associated with a phase transformation. It may be mentioned that the phase transformations in metals are normally associated with a sufficiently high cooling rate. The origin of the adiabatic cutting is not specified here. It is understood that in the case of geologic materials like concrete the mineral particles will erode a projectile surface (steel, for example).

The main mechanism assumed here which leads to evaluation of the surface thermodynamics and erosion is based on dynamic plasticity with thermal coupling. Although the plasticity-based models of friction are not new [15,16,17], the concept of applying adiabatic shear banding as a principal mechanism in friction analysis is relatively new [14].

In general, the surface topography can be represented as a set of vertical micro-asperities with randomly distributed highs h_n and with a constant square cross section. Such an idealization is shown in Fig.1. In this approximation three levels of micro-asperity heights can be recognized: first are the micro-asperities of the highest level (red), second are the (green) micro-asperities of the mean height, and finally there is the subset of the lowest micro-asperities (blue). The total number of asperities is N over the surface S, so the mean density of the regular array of micro-asperities with the mean square cross section A^2 is $n = N/S$. Since $S = N A^2$, the density of all micro-asperities is related to the mean side dimension A by the relation $n = 1/A^2$.

It is assumed that the idealized three subsets of micro-asperities have different functions during the sliding process. The subset with the highest micro-asperities is cut by adiabatic shear banding and at the same time it carries, to some extent, the normal stress. The medium subset supports the normal stress but is not cut. Finally, the subset with the shortest micro-asperities rests without contact. The highest micro-asperities produce the "hot spots" shown in red on the top view of the surface S in Fig.2.

The surface topography approximated by the random distribution of heights must involve a statistical analysis of the adiabatic cutting. It is too early to apply such an approach, and in the following analysis a simplified version of the asperity distribution has been assumed, that is, a uniformly distributed array, N_a, of the active micro-asperities of the equal height h which fail by adiabatic shearing. The elementary cell (active asperity) with the active micro-asperity is shown in Fig.3. In this approach the surface S is covered by a regular array of square

elementary cells (active asperities) with the mean dimension Λ, thus $S = N_a \Lambda^2$, and the density of such defined asperities is $n_a = 1/\Lambda^2$. Every elementary cell carries one vertical micro-asperity of the cross section a^2, which is cut by ASB. The elementary cell surface is only partly occupied by the active micro-asperity; the rest of the surface is filled by the lower-height micro-asperities invisible in this approximation. The fractional area of the active micro-asperities can be defined as follows [14],

$$f_a = \left(\frac{a}{\Lambda}\right)^2 \qquad f_a \leq 1 \tag{1}$$

In general, when three levels of height are assumed, the surface S is divided into three domains:

$$S = S_0 + S_a + S_b \tag{2}$$

where the S_0 domain is the surface with no contact, S_a and S_b are respectively the surfaces occupied by the active (adiabatic cutting) and passive (Coulomb friction) micro-asperities. Assuming a constant number, N, of all asperities, the relation between particular fractions is given by

$$1 = f_{n0}\, f_{s0} + f_{na}\, f_{sa} + f_{nb}\, f_{sb} \tag{3}$$

with

$$f_{n0} = \frac{N_o}{N}, \quad f_{s0} = \left(\frac{c}{A}\right)^2, \quad f_{na} = \frac{N_a}{N}, \quad f_{sa} = \left(\frac{a}{A}\right)^2, \quad f_{nb} = \frac{N_b}{N}, \quad f_{sb} = \left(\frac{b}{A}\right)^2$$

where b and c are the side dimensions of the micro-asperities with Coulomb friction and with no contact, respectively. Equation (3) can be rewritten in the form

$$1 = \left(\frac{a}{\Lambda_a}\right)^2 + \left(\frac{b}{\Lambda_b}\right)^2 + \left(\frac{c}{\Lambda_c}\right)^2 \tag{4}$$

where $\Lambda_a, \Lambda_b \; and \; \Lambda_c$ are, respectively, the mean distances between particular micro-asperities, or

$$1 = n_a\, a^2 + n_b\, b^2 + n_c\, c^2 \tag{5}$$

where n_a, n_b, n_c are the densities of the respective micro-asperities.. The surface fractions f_{sa} and f_{sb} are the geometry parameters of the problem. Assuming further that a = b = c, that is, $f_{sa} = f_{sb} = f_{s0}$, Eq.(3) becomes

$$1 = f_{sa}\left(f_{n0} + f_{na} + f_{nb}\right) \tag{6}$$

This last relation is important since the number fraction of the particular contacts, that is the active and Coulomb micro-asperities, changes as a function of pressure. An increase of pressure will increase the number of active micro-asperities while simultaneously diminishing those of the Coulomb-type. Introducing the principle of mixture and the influence function, p, of pressure (denoted as p(p)), Eq.(6) becomes

$$1 = f_{sa}\left[p(p) f_{na} + \left(1 - p(p)\right)\left(f_{n0} + f_{nb}\right)\right] \tag{7}$$

It is obvious that p(p) must be an increasing function of pressure. It is assumed in the simplified modeling that the effect of pressure is introduced through modification of Eq.(1) as follows:

$$f_a\left(\frac{a}{\Lambda_a}, p\right) = \left(\frac{a}{\Lambda_a}\right)^2 f_{na}\, p(p) \tag{8}$$

where $f_{na}\, p(p) = \dfrac{n_a(p)}{n}$, n_a/n is the density fraction of the active (adiabatic) micro-asperities, $0 < f_{na}\, p(p) < 1$, n is the total density of asperities. In this approach the area fraction remains constant but the density of the active micro-asperities should increase as a function of pressure. At the same time the mean distance Λ_a between the active micro-asperities decreases. The evolution of the density n_a is assumed in the form of the following differential equation

$$\frac{dn_a}{dp} = M - B n_a \tag{9}$$

This is a standard evolution equation when the neighbor entities slow down the growth rate of population; M is the constant characterizing the ability to growth of the active micro-asperities and B is the constant related to the probability of interaction between neighboring micro-asperities. The general solution of Eq.(9) is given by

$$p = -\frac{1}{B}\ln\left(M - B n_a\right) + C \tag{10}$$

The constant C can be found from the initial conditions $n_a = n_{a0}$ *when* $p = p_0$. The final form of the solution is

$$n_a(p) = \frac{M}{B} - \left(\frac{M}{B} - n_{a0}\right)\exp\left(-B(p - p_0)\right) \tag{11}$$

Limit of the solution is

$$\frac{\lim n_a}{p \to \infty} = n \quad and \quad n = \frac{M}{B} \tag{12}$$

Finally

$$\frac{n_a(p)}{n} = 1 - (1 - \frac{n_{a0}}{n})\exp\left(-B(p - p_0)\right) \tag{13}$$

The solution (13) can be introduced into Eq.(8), the final result is

$$f_a(\frac{a}{\Lambda_a}, p) = \left(\frac{a}{\Lambda_a}\right)^2 \left[1 - (1 - \frac{n_{a0}}{n})\exp\left(-B(p - p_0)\right)\right] \tag{14}$$

Equation (14) will be used later, in the different stages of this study, to calculate variety of parameters.

3. Coefficient of friction

By definition the coefficient of friction is the ratio of the mean tangential force $\overline{F}_x$ to the mean normal force $\overline{F}_y$, thus

$$\mu = \frac{\overline{F}_x}{\overline{F}_y} \tag{15}$$

Since two types of the micro-asperities in contact are assumed, "a" and "b", Eq.(15) can be rewritten as

$$\mu = \frac{F_{xa} + F_{xb}}{F_{ya} + F_{yb}} \tag{16}$$

Introducing tangential and normal stresses the mean forces are

$$\overline{F}_x = N_a a^2 \tau_a + N_b b^2 \tau_b \tag{17}$$

$$\overline{F}_y = N_a a^2 \sigma_a + N_b b^2 \sigma_b \tag{18}$$

where $\tau_a, \tau_b, \sigma_a, \sigma_b$ are shear and normal stresses on particular micro-asperities. Introducing Eqs.(17) and (18) into Eq.(15) together with the following approximations: a $\approx$ b,

$\tau_b = \mu_b \sigma_n$, that is the local Coulomb friction and $p = \sigma_a \approx \sigma_b$, that is the normal pressure the generalized coefficient of friction is given by

$$\mu = \frac{n_a(p)\tau_a}{p(n_a(p)+n_b(p))} + \mu_b \frac{n_b(p)}{n_a(p)+n_b(p)} \tag{19}$$

As expected, the total coefficient of friction in this model combines two terms, the first one is due to shear stress understood as an result of plastic deformation of the active micro-asperities, isothermal or adiabatic, the second one is due to standard Coulomb friction occurring in non-deformed plastically asperities. Because plasticity is rate-dependent, the shear stress and the generalized coefficient of friction must be a function of sliding velocity V. It is interesting to note that both terms depend on the normal pressure p. Since the population of the active micro-asperities increases as a function of pressure, as it is predicted by Eq.(13), and at the same time the Coulomb micro-asperities diminishes with the same proportion (total n assumed constant), in the limit, plasticity will dominate at high pressures. An inverse situation is expected for low normal pressure, the Coulomb friction will dominate. The next step in simplifications is to neglect the Coulomb friction and to analyze the plasticity term. Since $n = n_a + n_b$ Eq.(19) can be written as

$$\mu = \frac{n_a(p)\tau_a}{pn} \tag{20}$$

Introduction of Eq.(13) into Eq.(20) yields the coefficient of friction based on plasticity

$$\mu = \frac{\tau_a}{p}\left[1-(1-\frac{n_{a0}}{n})\exp(-B(p-p_0)\right] \tag{21}$$

However, in this approximation the shear stress is assumed as sliding resistance without specification of the fractional area of the elementary cell. The effective shear stress τ_{eff} should be reduced with the following proportion, [13],

$$\tau_a = \tau_{eff}\left(\frac{a}{\Lambda}\right)^2 \tag{22}$$

Finally, the coefficient of friction due to plasticity is given by

$$\mu = \frac{\tau}{p}\left(\frac{a}{\Lambda}\right)^2\left[1-(1-f_{a0})\exp(-B(p-p_0)\right] \tag{23}$$

with $f_{a0} = n_{a0}/n$ and the subscript *eff* is omitted. The most important part of this analysis is the ratio τ/p. It is assumed that the normal pressure p is a fraction x of the yield stress in compression σ_y, thus $p = x\sigma_y$ and Eq.(23) becomes

$$\mu = \frac{\tau}{x\sigma_y}\left(\frac{a}{\Lambda}\right)^2\left[1-(1-f_{a0})\exp\left(-Bx_0\sigma_y\left(\frac{x}{x_0}-1\right)\right)\right] \tag{24}$$

where $p_o = x_0\sigma_y$. In order to show the effect of the number of active contact points on μ the term in the square brackets was analyzed with the following initial conditions: $f_{ao} = 0.1$ for $x_o = 0.01$ and $f_{max} = 0.99$ for x = 1, $B = 5.04655*10^{-3}$, the result is shown in Fig.4. As expected, at high pressure the saturation level of the number of active asperities is reached.

The next important step is discussion of the ratio τ/σ_y. It is obvious that a yield condition must be introduced. Many possibilities can be envisaged. For example, in [11] the Prager-Ziegler kinematic hardening was assumed where shear stress is independent of the normal stress. However, if the Huber-Mises yield condition is assumed, that is $\tau_y = \sigma_y/\sqrt{3}$, and the shear stress is assumed to increase proportionally with the normal stress, that is $\tau = x\tau_y$, this results in a Coulomb-type equation, where the coefficient of friction is given by

$$\mu = \frac{1}{\sqrt{3}}\left(\frac{a}{\Lambda}\right)^2\left[1-(1-f_{a0})\exp\left(-\sqrt{3}Bx_0\tau_y\left(\frac{x}{x_0}-1\right)\right)\right] \tag{25}$$

The limit of the coefficient of friction is reached for x = 1 and then μ = 0.577 (for $a/\Lambda = 1$). The result of calculations for this model of friction, with τ_y = 520 MPa and for different fractional area, as a function of non-dimensional pressure is shown in Fig.5. Another possibility, a very probable one, is that the active micro-asperities are always plastified, that is $\tau = \tau_y$ and pressure increases in proportion to the yield stress, that is $p = \sqrt{3}x\tau_y$. This approach to the coefficient of friction, which should be rather called *friction parameter*, because the definition the coefficient of friction in the Coulomb sense is not obeyed, can be written as follows

$$\mu = \frac{1}{x\sqrt{3}}\left(\frac{a}{\Lambda}\right)^2\left[1-(1-f_{a0})\exp\left(-\sqrt{3}Bx_0\tau_y\left(\frac{x}{x_0}-1\right)\right)\right] \tag{26}$$

The result of the numerical calculation for the same conditions as in the previous case is shown in Fig.6. This time the friction parameter reaches relatively high values and substantially decreases as a function of pressure.

In conclusion, the ratio τ/p is a decisive variable in definition of "friction", or rather resistance to sliding, in all problems involving plasticity, visco-plasticity and temperature-coupled visco-plasticity. Experimental results collected in [15] and [16] clearly indicate that the resistance to sliding substantially diminishes when the sliding velocity increases. Further experimentation is of great importance, especially at very high sliding velocities, ie., above 100 m/s, to shed some light on dynamic resistance to friction.

4. Estimation of strain rates at high-velocity sliding

It is well known that at high strain rates all materials show very high rate sensitivity. The range of strain rates expected in a particular problem indicates a level of approximation needed in constitutive modeling. Since the heights h of the micro-asperities under consideration may be of an order in between few micrometers to say few tens of a millimeter and the whole range velocities of interest, say from 1.0 m/s to about 1500 m/s, the range of strain rates is very large. In order to estimate this range a simple calculation was performed, the results are shown in Fig.7 and Fig.8. The shear strain rate defined by standard relation

$$\dot{\Gamma} = \frac{V}{h} \tag{27}$$

The range of asperity heights is assumed as 5.0 μm to 100 μm (0.1 mm). In Fig.7 the velocity was assumed as low as 1.0 m/s and the range of strain rates is in between 10^4 1/s (h = 0.1 mm) and 10^6 1/s. The strain rates are surprisingly high even for sliding velocity as low as 1.0 m/s. Fig.8 shows the logarithm of strain rate in the of velocity range 200 m/s < V < 1600 m/s as function of micro-asperity heights. Again, strain rates are extremely high, from about 10^5 1/s (h = 0.1 mm) to about 10^8 1/s for smaller h.

The main conclusion reached on the basis of those calculations can be formulated in the following statement: *constitutive relations using standard dynamic plasticity cannot be applied to find the resistance to sliding friction at very high strain rates.* Alternatively,

constitutive relations based on pseudo-viscosity using electron or phonon viscosity and supersonic dislocations, or even hydrodynamic modeling, might prove useful.

5. Constitutive modeling at very high strain rates - pseudo-viscosity

It is commonly assumed in constitutive modeling of dynamic plasticity based on dislocation dynamics that at specific temperature the effective shear stress required to activate dislocation motion without assistance of thermal vibration of atoms is the limit of standard visco-plasticity approach. This level of shear stress is called the mechanical threshold, [18]. This mechanical threshold is reached at absolute zero temperature or at very high specific strain rate, typically ~5x10^3 1/s, then at T = 0 K, $\tau = \hat{\tau}_0$ *and* $\dot{\Gamma} = \dot{\Gamma}_{C0}$. Above the threshold strain rate $\dot{\Gamma}_{C0}$ there is an increase in defects (dislocations) together with a substantial increase of the mean dislocation velocity [19]. High dislocation velocity triggers different micro-mechanisms of plastic flow like electron or phonon viscosity, which leads to the rate-dependent threshold stress, [19]. In other words, when the applied stress τ exceeds the threshold stress, $\tau > \hat{\tau}$, T > 0, the dislocation velocity is controlled by energy dissipation via electron and phonon viscosities when dislocations move through the lattice. It is commonly assumed that this dissipation is linear and viscous and the force F acting on a mobile dislocation of length l_m is proportional to the mean dislocation velocity with the proportionality constant B called the viscous drag, such relations may be written as

$$F = B\bar{v} \qquad F = \tau l_m b \qquad l_m = 1/\sqrt{\rho_m} \tag{28}$$

where ρ_m and B are respectively the mobile dislocation density and viscous drag, τ the is shear stress on a dislocation, b is the magnitude of Burger's vector (b = 2.48x10^{-8} cm for iron). The Orowan relation relates $\dot{\Gamma}$, the shear strain rate, with the mobile dislocation density and the mean dislocation velocity

$$\dot{\Gamma} = b\,\rho_m\,\bar{v} \tag{29}$$

The shear stress can be written as

$$\tau = \tau_0 + \frac{B\bar{v}}{l_m b} \quad \text{or and} \quad \tau = \tau_0 + \frac{B}{b^2\sqrt{\rho_m}}\dot{\Gamma} \quad \text{with} \quad \eta = \frac{B}{b^2\sqrt{\rho_m}} \tag{30}$$

with η, the pseudo-viscosity. Finally, at strain rates higher than the threshold strain rate, and the threshold stress, the flow stress can be written as

$$\tau = \tau_0(T) + \eta(T)\dot{\Gamma} \tag{31}$$

The threshold stress and the pseudo viscosity must be temperature dependent, where T is the absolute temperature.

At very high strain rates dislocations approach supersonic velocity C_2, $C_2 = \sqrt{G/\rho_0}$, where G is the shear modulus and ρ_0 is the mass density. The supersonic approximation to the dislocation drag has been proposed in [19] in the form

$$F = \frac{B\bar{v}}{\left[1-(\frac{\bar{v}}{C_2})^2\right]^{1/2}} \quad \text{and} \quad \tau = \tau_0 + \frac{B\dot{\Gamma}}{b^2\sqrt{\rho_m}}\left[1-\left(\frac{\dot{\Gamma}}{b\,\rho_m C_2}\right)^2\right]^{-1/2} \tag{32}$$

with the critical strain rate $\dot{\Gamma}_{crit} = b\,\rho_m C_2$ and generalized pseudo-viscosity η, $\tau = \tau_0 + \eta\dot{\Gamma}$

$$\eta = \eta_0\left[1-\left(\frac{\dot{\Gamma}}{b\,\rho_m C_2}\right)^2\right]^{-1/2} \quad \text{with} \quad \eta_0 = \frac{B}{b^2\sqrt{\rho_m}} \tag{33}$$

It is interesting to analyze theoretical limits of the viscous drag approximation. Assuming the elastic wave speed in shear mode C_2 = 3.0 mm/μs the critical shear strain rate for iron may be estimated from the linear relation (Eq.(29)) $\dot{\Gamma}_{crit} = 7.44*10^{-3}\,\rho_m$, where $[\rho_m] = [1/cm^2]$. For example, for the mobile dislocation density 10^8 1/cm^2 the critical strain rate is $7.44*10^5$ 1/s and for 10^{10} 1/cm^2 the critical strain rate reaches value of $7.44*10^7$ 1/s. These estimations indicate that the strain rates during penetrator sliding are very close to the limiting strain rates predicted by the theory of dislocation dynamics. To complete this part of the analysis Eq.(33) has been analyzed for different values of the mobile dislocation density and the result is shown in Fig.9.

The value of η_0 was found from the direct impact shear experiments on mild steel, [19], and earlier experimental results, [21], which confirm the value of the pseudo-viscosity at 0 K, η_0 =

$2.65*10^3$ Pa*s. Theoretical curves show that the viscous approximation with the constant value of η_0 is correct at high densities of mobile dislocations, say above 10^8 1/cm^2.

Under this assumption Eq.(31) has been modified to account for the temperature effects

$$\tau(\Theta,\dot{\Gamma}) = \frac{G(\Theta)}{G_0}\hat{\tau}_0 + \eta(\Theta)\dot{\Gamma} \qquad \tau > \hat{\tau}_0 \tag{34}$$

where $\Theta = T/T_m$ is the homologous temperature and T_m is the melting point. Because the thermal softening of the crystalline lattice diminishes resistance to plastic flow, the mechanical threshold stress at $\Theta = 0$ ($T = 0$) is normalized by the relative changes of the shear modulus of elasticity as a function of temperature, G_0 is the shear modulus at $\Theta = 0$. In the literature many approximations to the relative changes of the shear modulus as a function of temperature have been proposed. Here, the simplest approximation that fits relatively well experimental data is introduced

$$\frac{G(\Theta)}{G_0} = 1 - \Theta^2 \qquad 0 < \Theta < 1 \tag{35}$$

An open question remains with regard to the temperature dependence of the pseudo-viscosity. In general, the pseudo-viscosity must be a decreasing function of the homologous temperature Θ. Since the surface temperatures of KE penetrators rapidly reach the melting point, an expression for the pseudo-viscosity must also take into account the viscosity of a liquid metal. The following phenomenological expression for $\eta(\Theta)$ satisfies such boundary conditions for temperature, that is at $\Theta = 0$, $\eta(0) = \eta_0$ and at $\Theta = 1$, $\eta(1) = \eta_m$

$$\frac{\eta(\Theta)}{\eta_0} = \frac{1}{2}\left[1 - \tanh(A\Theta - B)\right] \tag{36}$$

where A and B are constants. Values of the constants that satisfy the boundary conditions are A = 4, B = 2. The relative changes of the pseudo-viscosity as a function of the homologous temperature is shown in Fig.10. The model is based on the ideal plasticity concept (no strain hardening) and both relative functions, i.e. the shear modulus and the pseudo-viscosity, are a rapidly decreasing function of the homologous temperature.

6. Thermal coupling in adiabatic conditions

It has been known for a long time that the large part of the work of plastic deformation (on average 90%) is converted into heat. In the 19th century Tresca remarked on "heat lines" which appear during forging. An adiabatic process of plastic deformation occurs when the heat conduction between neighboring particles and surroundings is suppressed. A specific case of the adiabatic process of plastic deformation occurs under condition of normal heat conduction, but at high strain rates, when the deformation process is too short to permit significant heat transfer in the crystalline lattice. Adiabatic deformation triggers a specific instability called Adiabatic Shear Band, discussed in the section 1 of this study. Many papers have been published on occurrence of the ASBs, theoretical, experimental and numerical. It is out of scope of this paper to review them. However, one of the earliest detailed analysis of adiabatic process of deformation and analysis of the stability conditions in tension can be found in [22].

The equation of heat conduction in the form applicable to dynamic plasticity may be written as

$$\rho C_v \frac{\partial T}{\partial t} = \beta \tau(\Gamma, \dot{\Gamma}, T) \frac{\partial \Gamma}{\partial t} - \lambda \frac{\partial^2 T}{\partial y^2} \tag{37}$$

where y is the direction of the heat conduction, ρ, C_v and λ are respectively the mass density, the specific heat at constant volume and the heat conductivity constant (Fourier constant), β is the fraction of the plastic work converted into heat, $\beta \approx 0.9$. In case of $\lambda = 0$ the process is adiabatic. When the homologous temperature is introduced, and the strain hardening is neglected, the energy balance equation, Eq.(37), is transformed into the following form

$$\frac{\partial \Theta}{\partial t} = \frac{\beta}{\rho C_v T_m} \tau(\dot{\Gamma}, \Theta) \frac{\partial \Gamma}{\partial t} - \frac{\lambda}{\rho C_v} \frac{\partial^2 \Theta}{\partial y^2} \tag{38}$$

Introducing constitutive relations (34), (35) and (36) into the equation of heat conduction the estimation of the Heat Affected Zone (HAZ) can be found numerically. In case of the adiabatic process Eq.(38) is reduced to the following form, [22],

$$\frac{d\Theta}{d\Gamma} = \frac{\beta}{\rho C_v T_m} \tau(\dot{\Gamma}, \Theta) \tag{39}$$

This simple ordinary differential equation should be integrated with the initial conditions $\Theta = \Theta_0$ for $\Gamma = 0$. Since the simplified constitutive relations do not depend on strain the separation of variables and integration is direct. Transition from the isothermal into adiabatic process of deformation was analyzed numerically for a short thin tube deformed in torsion at different rates. For steel the "50%" transition from isothermal to adiabatic deformation was found to occur at $\dot{\Gamma} \approx 40 \quad 1/s$. No doubt, at strain rates higher than 100 1/s the process of deformation is entirely adiabatic.

7. Temperature evolution in one micro-asperity

Assume, as the first approximation, that the micro-asperity is in adiabatic state, and over the height h shear deformation is uniform. Thus, in fact, only one layer of equal micro-asperities is analyzed. Assume further that the height has the same dimension in all calculations, h = 20 μm, a mean value of ASB thickness observed experimentally. Widths of so called "transformed" ASB varies in steel from ~5.0 μm to ~20.0 μm, non-transformed band thickness varies from ~20.0 μm to even 100 μm. The scheme assumed in numerical calculations is shown in Fig.11 where the micro-asperity is deformed in shear to the critical failure strain Γ_c. The point of shear serves as the source of a fast increase of temperature, usually up to the melting level.

It is of interest to calculate the time interval it takes the homologous temperature to reach the melting point or failure at a particular velocity of sliding V. Equation (39) can be written as

$$d\Theta = \frac{\beta}{\rho C_v T_m} \tau_0 \left[\left\langle 1 - \Theta^2 \right\rangle + \frac{\eta_0}{2\tau_0 h} f_\eta(\Theta) V \right] \frac{V}{h} dt \tag{40}$$

with

$$f_\eta(\Theta) = 1 - \tanh\left[2(2\Theta - 1)\right] \tag{41}$$

where $\dot{\Gamma} = V/h$, and the operator $\langle * \rangle$ introduced into Eq.(40) means that if $\Theta^2 > 1$ then $\left\langle 1 - \Theta^2 \right\rangle = 0$ otherwise $1\text{-}\Theta^2$. If the failure criterion in shear is assumed as the critical shear

strain Γ_f, the time interval to failure is given by $t_f = h\Gamma_f / V$. Now Eq.(40) can be integrated and the interval of time t_i found for a specified value of the homologous temperature Θ_i

$$t_i = \int_{\Theta_0}^{\Theta_i} \frac{d\Theta}{C_1 \tau_0 \left[\left\langle 1-\Theta^2 \right\rangle + \frac{\eta_0 V}{2\tau_0 h} f_\eta(\Theta) \right] \frac{V}{h}} \qquad C_1 = \frac{\beta}{\rho C_v T_m} \tag{42}$$

Of course, the most important parameter of the problem is the imposed velocity V. The set of equations has been analyzed numerically with the following values of constants

$\Theta_0 = 0.1628$ that is $\Theta_0 = 293$ K/1800 K, $T_m = 1800$ K for iron

$\beta = 0.9$

$\rho = 7800$ kg/m^3

$C_v = 500$ J/kg K so $C_1 = 1.282052*10^{-10}$ m^2/N

$h = 20.0$ μm

$\tau_o = 520$ MPa , this value of the mechanical threshold at $\Theta = 0$ is estimated from the experimental data for 1018 steel given in [20]

$\eta_o = 2.65*10^3$ Pa*s, this value of the pseudo-viscosity at $\Theta = 0$ is estimated from the experimental data for a mild steel, [20,21], $\eta_{RT} = 2.5*10^3$ Pa*s

The results of calculations are shown in Fig12, Fig.13 and Fig.14. The time to reach particular homologous temperature Θ for different velocity level V is shown in Fig.12a, b and 12c.Three velocity ranges were calculated: (a) 1.0 m/s< V <10 m/s; (b) 10 m/s < V< 100 m/s and (c) 100 m/s < V < 1000 m/s. It is clear that the melting point is reached very quickly, for velocity 10 m/s the melting point is reached after about 40 μs, for V = 100 m/s after about 0.8 μs and for V = 1000 m/s after about 10 ns (1 ns = 10^{-9} s). In conclusion, the active micro-asperities reach almost instantaneously the melting temperature. Different view of the numerical results are shown in Fig.13 a, b and c. The time to reach particular homologous temperature has been calculated for three different ranges of velocities. Again, the range of times to reach particular homologous temperature diminishes rapidly with velocity. An interesting question arises, what is reached first failure or melting? The mechanical failure criterion defined by $t_c = h\Gamma_c / V$ may be satisfied before the melting temperature is reached. The results of such analysis are shown in Fig14 a, b and c in the form of time to reach failure criterion with the critical shear strain $\Gamma_c = 2.0$ or the melting temperature. At low and medium-high velocities

the failure dominates, however at velocities higher than about 200 m/s (see Fig.14c) the melting point is reached earlier than failure.

8. Heat Affected Zone (HAZ)

The evolution of temperature calculated for one micro-asperity is one of the heat sources that heats the bulk material. Other heat sources may be in the form of micro-debris rubbing the surface and also foreign grains of perforated material. During penetration the bulk material is constantly heated by repeated process of adiabatic shearing of micro-asperities. The failure of micro-asperities is repeated with a high frequency and every new failure contributes as a "hot point" to the increase of temperature of the bulk material. The process is ended after time $t_p = L_p/V$, where L_p is the projectile length. It is interesting to calculate the frequency of cutting. Assuming the critical strain to failure $\Gamma_c = 2.0$ and the micro-asperity height h = 20 μm the frequency of cutting is $\nu_c = V/(h\,\Gamma_c)$, for V = 100 m/s the frequency of cutting is ν_c = 2.5 MHz, for V = 1000 m/s the frequency reaches ν_c = 25 MHz. With this frequency, the bulk surface is heated practically all the time by the melt on the surface. In order to estimate the HAZ the heat conduction equation should be solved, Eq.(38), with the boundary conditions $\Theta = 1$ on the bulk surface (y = 0) and $\Theta = \Theta_o$ inside the bulk material (for steel $\Theta_o = 0.1628$) the initial conditions are $\Theta = \Theta_o$ for t = 0. A simplified estimation of HAZ has been proposed in [14]. With the process time t_p ,which is the characteristic time of the heat conduction, the HAZ is estimated as a characteristic thermal diffusion length during that time. The result is

$$H = \frac{1}{\alpha}\left(\frac{\lambda}{\rho C_v}\frac{L_p}{V}\right)^{1/2} \tag{43}$$

where H denotes the HAZ and α is the characteristic constants of the problem considered. Constant α has been discussed in [14] and estimated as $\alpha = 1/\sqrt{2\pi}$ on the basis of the solution of the similar boundary value problem reported in [23]. It is interesting to note that for a constant projectile length the thickness of the HAZ diminishes in proportion to $1/\sqrt{V}$. Assuming thermal conductivity constant λ = 54.0 W/m K (steel) the size of HAZ has been calculated as a function of the penetration time $t_p = L_p/V$ the results are shown in Fig.15. The upper part shows HAZ in millimeters for relatively long time of penetration, the lower figure

for the short times. For example, when L_p is assumed 500 mm and velocity 100 m/s the penetration time is relatively long, t_p = 5.0 milliseconds, for L_p = 100 mm and V = 1500 m/s, t_p = 66.7 microseconds. The estimation of HAZ gives the dimension range from about 200 μm to about 5 mm. This estimation is not directly related to so the called transformed zone. The transformed zone should be in general related to the cooling rate of a material. The transformed zone must be thinner in comparison to the present estimates of HAZ.

9. Estimation of the bulk material temperature

Since the HAZ is approximated by Eq.(43) a simple method can be used to approximate the bulk material temperature, [14]. The energy balance between the input energy produced by the active micro-asperities and the absorbed energy by the HAZ per unit time and over the surface S leads to the following relation

$$\rho C_v (T_b - T_0) S H = \beta \tau(V,T) V \left(\frac{a}{\Lambda}\right)^2 \left(\frac{n_0(p)}{n}\right) S t_p \tag{44}$$

where $\Delta T = T_b - T_0$ is the increment of temperature due to the heat production by the active micro-asperities. Introducing expression for H (Eq.(43)) into Eq.(44) the energy balance becomes

$$\Theta_b = \Theta_0 + \frac{\alpha \beta}{T_m}\left(\frac{L_p}{\lambda \rho C_v}\right)^{1/2}\left(\frac{a}{\Lambda}\right)^2 f_a\left(\frac{a}{\Lambda}, p\right)\tau(\Theta_b, \dot{\Gamma})\, V^{1/2} \tag{45}$$

Equation (45) must be solved for Θ_b after introduction of Eq.(14) also Eqs(34),(35) and (36). Analytic solution is possible only for a constant viscosity η. Denoting the following expressions in Eq.(45) as

$$D(V, p, L_p, \frac{a}{\Lambda}) = \frac{\alpha \beta \tau_0}{T_m}\left(\frac{L_p}{\lambda \rho C_v}\right)^{1/2}\left(\frac{a}{\Lambda}\right)^2 f_a\left(\frac{a}{\Lambda}, p\right) V^{1/2}$$

$$E(V,\eta) = \frac{\eta}{\tau_0}\frac{V}{h}$$

the simplified notation of Eq.(45) is obtained

$$\Theta_b = \Theta_0 + D(1 - \Theta_b^2 + E) \tag{46}$$

The final form to be solved is in the quadratic equation

$$\Theta_b^2 + \frac{\Theta_b}{D} - \left(\frac{\Theta_0}{D} + F\right) = 0 \qquad \eta=\text{const} \tag{47}$$

with $F = 1 + E$.

The solution of Eq.(47) is

$$(\Theta_b)_{1,2} = \frac{1}{2D}\left[\pm(1 + 4D(\Theta_0 + DF))^{1/2} - 1\right] \tag{48}$$

The solution has been analyzed within the lower range of velocities for nine fractional areas and $f_{na} = 0.9$. The results are shown in Fig.16. The other parameters were assumed as follows: $\alpha\beta = 0.14324$, $\tau_0 = 520$ MPa, $L_p = 250$ mm, $\eta = 2.5*10^3$ Pa*s, h = 20 μm. The other constants are given in the previous parts of this paper. The explicit solution shows a very rapid increase of temperature, that is the melting point is reached very quickly. The main reason is the constancy of the pseudo-viscosity, the main generator of heat. Although the analytic solution may be understood as the upper bound of temperature increase, a complete analysis with $\eta(\Theta)$ can provide a more exact temperature evolution in the bulk material.

The results of such a complete analysis, which involves Eqs(14),(34),(35),(36) and Eq.(45) are shown in Fig.17. The roots of Eq.(45) were calculated as a function of velocity for four ranges, that is $0 < V < 1.0$ m/s, Fig17a ; 1.0 m/s $< V < 10$ m/s, Fig17b; 10 m/s $< V < 100$ m/s, Fig.17c and 100 m/s $< V < 1000$ m/s, Fig17d. A very consistent result has been found, the homologous temperatures increase steadily as a function of velocity up to different levels of saturation depending on the fractional area of micro-asperities. At velocities higher than 10 m/s the saturation levels of the homologous temperatures are close to or slightly above the melting point ($\Theta = 1$). Within the velocity range 100 m/s $< V < 1000$ m/s the homologous temperatures are higher than the melting point because the viscosity itself, this time real, produces heat. Of course, the picture is of qualitative nature since a true viscosity of melted steel is unknown at present. However, the trends presented in Fig.17 are in complete agreement with the physical intuition.

Further calculations show changes of the bulk temperature as a function of the fractional area a/Λ (asperity ratio) at different velocities. The results are shown in Fig18a, b and c for three different ranges of speeds. The fractional area has an important influence on the temperature evolution in the bulk material. If the fractional area is larger the heat transfer from the micro-asperities is more intense. Again, the temperatures of the melting point and above

are reached very quickly when the fractional area is increased. At very high velocities the effect of the fractional area is reduced.

10. Calculation of friction

The fundamental mathematical formula for the coefficient of friction μ is given by Eq.(23). By substituting for $\tau(\Theta,\dot{\Gamma})$ from Eqs(34), (35) and (36) an explicit formula for μ is obtained

$$\mu = \frac{\tau_0}{p}\left(\frac{a}{\Lambda}\right)^2\left[\left\langle\, 1-(\Theta_b(V))^2 \,\right\rangle + \frac{\eta(\Theta_b)V}{\tau_0 h}\right]\left[1-(1-f_{a0})\exp(-B(p-p_0)\right] \qquad (49)$$

where the operator $\langle * \rangle = 0$ *if* $\Theta \geq 1$ otherwise $\langle * \rangle = 1-\Theta_b^2$. The solution for $\Theta_b(V)$ is given by Eq.(48) and $\eta(\Theta_b)$ by Eq.(36).

In order to analyze the effect of sliding velocity on the coefficient of friction Eq.(49) was normalized by the coefficient of friction at the reference velocity V = 1.0 m/s. The ratio of the coefficients of friction R_μ is given by

$$R_\mu(V)_b = \frac{1-\Theta_b^2(V)+\eta(\Theta)V/\tau_0 h}{1-\Theta_{b0}^2(V_0)+\eta_0(\Theta)V_0/\tau_0 h} \qquad (50)$$

where V_0 = 1.0 m/s, $\Theta_{b0}(V_0)$ and $\eta_0(\Theta)$ denotes respectively the evolution of the homologous temperature and pseudo-viscosity at the reference velocity V_0 = 1.0 m/s. The ratio has been analyzed numerically and the results are shown in Fig.19, a, b, and c for different ranges of velocity. It is interesting to note that the ratio does not depend upon τ_0 / p. As expected, because of thermal coupling of mechanical properties, the ratio diminishes when velocity increases. This trend is directly due to the temperature softening of the flow stress. At very high velocities the ratio reaches very low values, at V = 1000 m/s the asymptotic value is less than 10% in comparison to the ratio at V = 1.0 m/s. The same trend is shown in Fig.20 where the ratio of the coefficients of friction is shown as a function of the nominal strain rate $\dot{\Gamma} = V/h$ in the logarithmic scale. The asperity size h = 20 μm combined with velocities V from 1.0 m/s to 1000 m/s yields extremely high strain rates, from 10^4 1/s to 10^7 1/s. Those calculations were performed for different fractional area, from 0.2 to 0.9 and for constant non-dimensional pressure 0.9.

A general definition of the coefficient of friction which stems from the asperity model is given by Eq.(19). The simplifications discussed previously have lead to the definition of the coefficient of friction based on plasticity in the form of Eq.(23). The most important part of the analysis is the question how to introduce the ratio τ / p. When the visco-plasticity is introduced in Eq.(23) in the form of the constitutive relations derived in this study, Eqs (34), (35) and (36), the ratio τ / p becomes strain-rate and temperature dependent.

Three possibilities based on plasticity are discussed below.

1. According to the Coulomb hypothesis the tangential force (shear stress) increases proportionally to the normal force (normal stress). Thus, $\tau = x\,\tau_y$ and $p = x\,\sigma_y$, $0 < x < 1$, and assuming the Huber-Mises yield condition (isotropic hardening), $\sigma_y = \sqrt{3}\,\tau_y$, the ratio τ / p is reduced to $\tau / p = 1/\sqrt{3}$ *or* $\tau / p = 0.577$. Thus, the upper limit of the coefficient of Coulomb friction based on isotropic plasticity is 0.577.
2. Another possibility introduced in [14] is the kinematic hardening where the yield surface is translated in the direction of plastic flow, that is in the direction of shear. This is the Prager-Ziegler hardening. Then, the ratio $\tau / p = \tau / \sigma_y$, with σ_y = const.
3. The last possibility considered in this study is an assumption that the pressure p increases proportionally to the yield stress, $p = x\,\sigma_y$, and shear stress remains at the threshold level τ_0. Again, the Huber-Mises yield condition is applied. The main physical motivation is that independently of the level of the normal stress the micro -asperities are always cut by adiabatic shearing.

Those three cases lead only to different initial levels of the coefficient of friction and different effect of pressure, but they *do not change the* general trends of how the coefficient of friction evolves when the velocity of sliding increases.

For cases 1 and 3 the equation for μ, (Eq.(49)), is reduced to the following forms

$$\mu = \frac{1}{\sqrt{3}}(*) \qquad \text{for case 1}$$

and

$$\mu = \frac{1}{\sqrt{3}\,x}(*) \qquad \text{for case 3}$$

where (*) is the multiplicative term after τ_0 / p in Eq.(49). When the following variables are introduced: $p = x\sqrt{3}\,\tau_0$ *and* $p_0 = x_0\sqrt{3}\,\tau_0$ in Eq.(49), the explicit expression for μ (case 3) is obtained

$$\mu = \frac{1}{\sqrt{3}\,x}\left(\frac{a}{\Lambda}\right)^2\left[\left\langle 1-(\Theta_b(V))^2\right\rangle + \frac{\eta(\Theta_b)V}{\tau_0 h}\right]\left\{1-(1-f_{a0})\exp\left[-Bx_0\sqrt{3}\,\tau_0\left(\frac{x}{x_0}-1\right)\right]\right\} \quad (51)$$

Both expressions for μ , the first one called coefficient of friction (Coulomb sense), and the second, called friction parameter, Eq.(51), have been evaluated numerically. The solution for Θ_b , that is Eq.(48), was introduced into Eq.(49) or Eq.(51) in order to find μ. In Fig 21 are shown the results of such calculations for the case of Coulomb plasticity where the coefficient of friction was calculated at different velocity levels, i.e.,: 1.0 m/s < V < 1000 m/s, as a function of non-dimensional pressure x/x_0 and for constant fractional area 0.9. As in the quasi-static case this coefficient of friction increases when pressure increases as well. However, at high sliding velocities the coefficient of friction remains almost constant at a very low level, independently of pressure. The most important results are shown in Fig.22 where the coefficient of friction, in the sense of Coulomb plasticity, is shown within three ranges of sliding velocity, (a) 1.0 m/s < V < 10 m/s, (b) 10 m/s < V < 100 m/s and (c) 100 m/s < V < 1000 m/s. Calculations were performed for different fractional area from 0.2 to 0.9 and at constant non-dimensional pressure 0.9. The level of the coefficient of friction at low velocities is relatively low, around 0.04 at V = 10 m/s. A substantial decrease in the coefficient of friction is observed at high sliding velocities . This is in complete agreement with the physical intuition and literature data. At velocity V = 1000 m/s an asymptotic value of μ is reached around 0.005. Overall the low values of the coefficient of friction is due to multiplication of the particular effects in the normalized form, that is all fractions are less than one and they are multiplied.

Another series of calculations have been performed to analyze the friction parameter (non Coulomb friction) defined by Eq.(51). In this case the friction parameter is decreasing function of non-dimensional pressure. This is shown in Fig.23 where the friction parameter is drawn at different velocities, 1.0 m/s < V < 1000 m/s, and at constant fractional area 0.9. The result that the friction decreases with pressure is consistent with experimental findings, for example [24]. The following series of calculations was similar as for the Coulomb plasticity

series, with the same three ranges of velocities from 1.0 m/s to 1000 m/s. The results are shown in Fig.24, (a) 1.0 m/s < V < 10 m/s, (b) 10 m/s < V < 100 m/s and (c) 100 m/s < V < 1000 m/s. Since the non-dimensional pressure was assumed in both cases at the same level 0.9 and assumed values of the fractional area were the same, from 0.2 to 0.9, changes of the friction parameter as a function of velocity are very similar for both cases. Because the absolute values of the coefficient of friction, and friction parameter, predicted by this model are relatively low and their evolution as a function of velocity seems to be correct the only solution at this stage of study is to introduce a phenomenological quasi-static coefficient of friction μ_0 determined at V = 1.0 m/s, or assume another low velocity of sliding. Estimation of the adjusted values of the coefficient of friction is provided for all definitions of τ / p by the expression

$$\mu = \mu_0 (*) \tag{52}$$

where (*) is the multiplicative term in Eq.(49) or Eq.(51).

In conclusion, the trend in evolution of friction as a function of velocity depends in both cases upon constitutive relations coupled with thermodynamics of HAZ defined as the time evolution of Θ_b.

11. Discussion and conclusions

After analysis presented in the previous chapters of this study, it appears that one of the most difficult problems in the mechanics of KE projectiles penetrating geological or cementitious target materials is a proper understanding of the frictional properties between the projectile surface and the target. The model developed in this study is limited to a very simple definition of the state of the projectile surface as a set of uniformly distributed micro-asperities with the same active height h = 20 μm. Of course, more general statistical models of micro-asperities of different heights can be envisaged, but such an approach is at present premature. The simplest way to approach such a difficult problem is to use fundamental laws of physics. In this case a physically based constitutive relation has been proposed. The main problem in this study was lack of experimental data on visco-plastic behavior of steels at very high strain rates, up to $5*10^7$ 1/s and at temperatures higher than half of the melting point. It

appears that this area of testing would be very useful in providing new data for further applications.

Although the heat conduction equation has not been solved numerically in this study, a useful approximation of the evolution of temperature in the bulk material was used after [14]. This approximation permitted finding the closed form solution for Θ_b. Because evolution of the bulk temperature could be estimated it also permitted finding the evolution of the coefficient of friction as a function of the sliding velocity. For every definition of the coefficient of friction a substantial decrease of the resistance to sliding has been found. This is consistent with the physical interpretation because a thin melted layer of metal on the projectile surface provides lubrication. An open question remains as to the role of the hydrostatic pressure. The experimental data reported in [24] seem to indicate that the hydrostatic pressure reduces friction. In Fig.25 are shown the re-analyzed results of the pin-on-disk experiments reported in [24] for projectile steel on gun steel. The coefficient of friction was determined as a function of velocity multiplied by pressure. For example, the experimental data suggests that at constant velocity the coefficient of friction will diminish as a function of pressure as predicted by Eq.(51). Thus, an advantage of the model presented here is that the hydrostatic pressure can be taken into consideration in a correct way. The physical limit of pressure is the yield stress, $\sigma_y = \sqrt{3}\,\tau_0$, with $\tau_0 = 520$ MPa the maximum pressure is about 9 kbar. Above this pressure level the pressure effect in the model becomes empirical. Albeit implementation of the friction model in the form of Eq.(51) into numerical codes is rather a too early move, preliminary trials should be recommended.

Acknowledgement/Disclaimer

This work was sponsored (in part) by the Air Force Office of Scientific Research, USAF, and under grant/contract number F49620-00-0288. The views and conclusions contained herein are those of the author and should not be interpreted or implied, of the Air Force Office of Scientific Research or the US Government.

The author wishes to acknowledge the numerous discussions with Drs. Mary Hughes and David Jerome, also with Mr. Odin Toness, all of AFRL-MNMW.

References

[1] Forrestal MJ, Frew DJ, Hanchak SJ, Brar NS. Penetration of grout and concrete targets with ogive-nose steel projectiles, Int. J. Impact Engng 1996; 18: 465.

[2] Beissel SR, Johnson GR. An abrasion algorithm for projectile mass loss during penetration, Int. J. Impact Engng 2000; 24: 103.

[3] Jones SE, Rule WK. On the optimal nose geometry for a rigid penetrator, including the effects of pressure-dependent friction, Int. J. Impact Engng 2000; 24: 403.

[4] Bai YL, Dodd B. Adiabatic Shear Localization, Pergamon Press, Oxford, 1992.

[5] Molinari A, Clifton RJ. Analytical characterization of shear localization in thermoplastic materials, ASME J. Appl. Mech., 1987; 54: 806.

[6] Marchand A, Duffy J. An experimental study of the formation process of adiabatic shear bands in a structural steel, J. Mech. Phys. Solids, 1988; 36: 251.

[7] Klepaczko JR, Lipinski P, Molinari A. An analysis of the thermoplastic catastrophic shear in some metals, Impact Loading and Dynamic Behaviour of Materials, DGM Informationsgessellschaft Verlag, Oberursel, 1988; (2): 69.

[8] Batra RC, Kim CH. Effect of thermal conductivity on the initiation, growth and bandwidth of adiabatic shear bands, Int. J. Eng Sci. 1991; 29: 949.

[9] Shawki TG. The phenomenon of shear strain localization in dynamic viscoplasticity, Appl. Mech. Rev., 1992; 45: S46.

[10] Klepaczko JR, Rezaig B. A numerical study of adiabatic shear banding in mild steel by dislocation mechanics based constitutive relations, Mech. of Materials, 1996; 24: 125.

[11] Klepaczko JR. Experimental investigation of adiabatic shear banding at different impact velocities, Final Techn. Report, US Army Eur. Res. Office, DAJA 49-90-C-0052, LPMM, Metz University, France, 1991.

[12] Klepaczko JR. On the critical impact velocity in plastic shearing, Metallurgical and Materials Application of Shock-Wave and High-Strain Rate Phenomena, Elsevier Sci. 1995: 413.

[13] Klepaczko JR, Klosak M. Numerical study of the critical impact velocity in shear, Eur. J. Mech., A/Solids1999; 18: 93.

[14] Molinari A, Estrin Y, Mercier S. Dependence of the Coefficient of friction on the sliding conditions in the high velocity range, ASME J. of Tribology, 1999; 121: 35.

[15] Lim SC, Ashby MF. Wear mechanism maps, Acta Metall. 1987; 35: 1.

[16] Lim SC, Ashby MF, Brunton JH. The effect of sliding conditions on the dry friction of Metals, Acta Metall. 1989; 37: 767.

[17] Ringey DA, Hirth JP. Plastic deformation and sliding friction and wear, Wear 1979; 53: 345.

[18] Kocks UF, Argon AS, Ashby MF. Thermodynamics and Kinetics of Slip, Pergamon Press, Oxford, 1975.

[19] Gilman J.J. Micromechanics of Flow of Solids, Mc Graw Hill, N.Y. 1969.

[20] Klepaczko JR. An experimental technique for shear testing at high and very high strain rates. The case of mild steel, Int. J. Impact Engng 1994; 15: 25.

[21] Campbell JD, FergussonWG. The temperature and strain-rate dependence of the shear strength of mild steel, Phil. Mag. 1970; 21: 63.

[22] Klepaczko JR. Generalized conditions for stability in tension test, Int. J. Mech. Sci. 1968; 10: 297.

[23] Carslaw HS, Jaeger JC. Conduction of heat in solids, Clarendon Press, Oxford,1959.

[24] Montgomery RS. Friction and wear at high sliding speeds, Wear 1976; 36: 275.

Figure captions

Fig.1 Approximation of surface topography by regular array of columns with random array of heights.

Fig.2 Top view of the surface topography, the hot spots are randomly distributed.

Fig.3 Elementary cell with an active micro-asperity which is cut by adiabatic shear band.

Fig.4 Non-dimensional number of contacts as a function of non-dimensional pressure, Eq. (22).

Fig.5 Quasi-static coefficient of friction (Coulomb type) as a function of non-dimensional pressure for different fractional area of elementary cell, Eq.(23).

Fig.6 Quasi-static friction parameter (non-Coulomb type) as a function of non-dimensional pressure, Eq.(24).

Fig.7 Logarithm of shear strain rate versus asperity height h, velocity of sliding 1.0 m/s.

Fig.8 Logarithm of shear strain rate versus asperity height at high velocities, 200 m/s < V < 1600 m/s.

Fig.9 Theoretical values of pseudo viscosity near the supersonic speed of dislocations.

Fig.10 Changes of the relative pseudo viscosity as a function of homologous temperature, Eq.(34).

Fig.11 Failure of a micro-asperity by ASB in elementary cell.

Fig.12 Time to reach specific homologous temperature for different ranges of velocity, (a) 1.0 m/s < V < 10.0 m/s, (b) 10 m/s < V < 100 m/s, (c) 100 m/s < V < 1000 m/s.

Fig.13 Time to reach specific homologous temperature as a function of velocity, (a), (b), (c) the same velocity ranges as in Fig.12.

Fig.14 Verification of the failure criterion for different ranges of velocities, (a),(b),(c) - the same velocity ranges as in Fig.12.

Fig.15 Heat affected zone (HAZ) for two different time scales.

Fig.16 Evolution of the bulk homologous temperature as a function of the sliding velocity for temperature-independent pseudo-viscosity.

Fig.17 Evolution of the bulk homologous temperature as a function of sliding velocity, complete temperature coupling; (a) 0 < V < 1.0 m/s, (b) 1.0 m/s < V < 10 m/s, (b) 10 m/s < V < 100 m/s, (d) 100 m/s < V < 1000 m/s.

Fig.18 Evolution of the bulk homologous temperature as a function of the fractional area of asperity a / Λ, (a) 1.0 m/s < V < 10 m/s, (b) 10 m/s < V < 100 m/s, (c) 100 m/s < V < 1000 m/s.

Fig.19 Ratio of the coefficients of friction for three ranges of velocities, (a) 1.0 m/s < V < 10 m/s, (b) 10 m/s < V < 100 m/s, (c) 100 m/s < V < 1000 m/s.

Fig.20 Ratio of the coefficients of friction as a function of the nominal strain rate at different fractional area and constant pressure.

Fig.21 Coefficient of friction, in the sense of Coulomb plasticity, as a function of the non-dimensional pressure at different levels of velocity and constant fractional area 0.9, range of velocities: 1.0 m/s < V < 1000 m/s.

Fig.22 Coefficient of friction, in the sense of Coulomb plasticity, as a function of sliding velocity V for different levels of fractional area and constant non-dimensional pressure, (a) 1.0 m/s < V < 10 m/s, (b) 10 m/s < V < 100 m/s, (c) 100 m/s < V < 1000 m/s.

Fig.23 Friction parameter (non-Coulomb friction) as a function of the non-dimensional pressure for different levels of velocity and constant fractional area 0.9, range of velocities: 1.0 m/s < V < 1000 m/s.

Fig.24 Friction parameter (non-Coulomb friction) as a function of sliding velocity V for different levels of fractional area and constant non-dimensional pressure, (a) 1.0 m/s < V < 10 m/s, (b) 10 m/s < V < 100 m/s, (c) 100 m/s < V < 1000 m/s.

Fig.25 Re-analyzed data for friction coefficient reported in [24] determined for projectile steel on gun steel by high speed pin-on-disk device; range of pressure 0.24 kbar < p < 1.34 kbar, range of velocity 3.0 m/s < V < 550 m/s.

$N := 20 \quad i := 1..20 \quad j := 1..20$

$f(x,y) := |md(1)|$

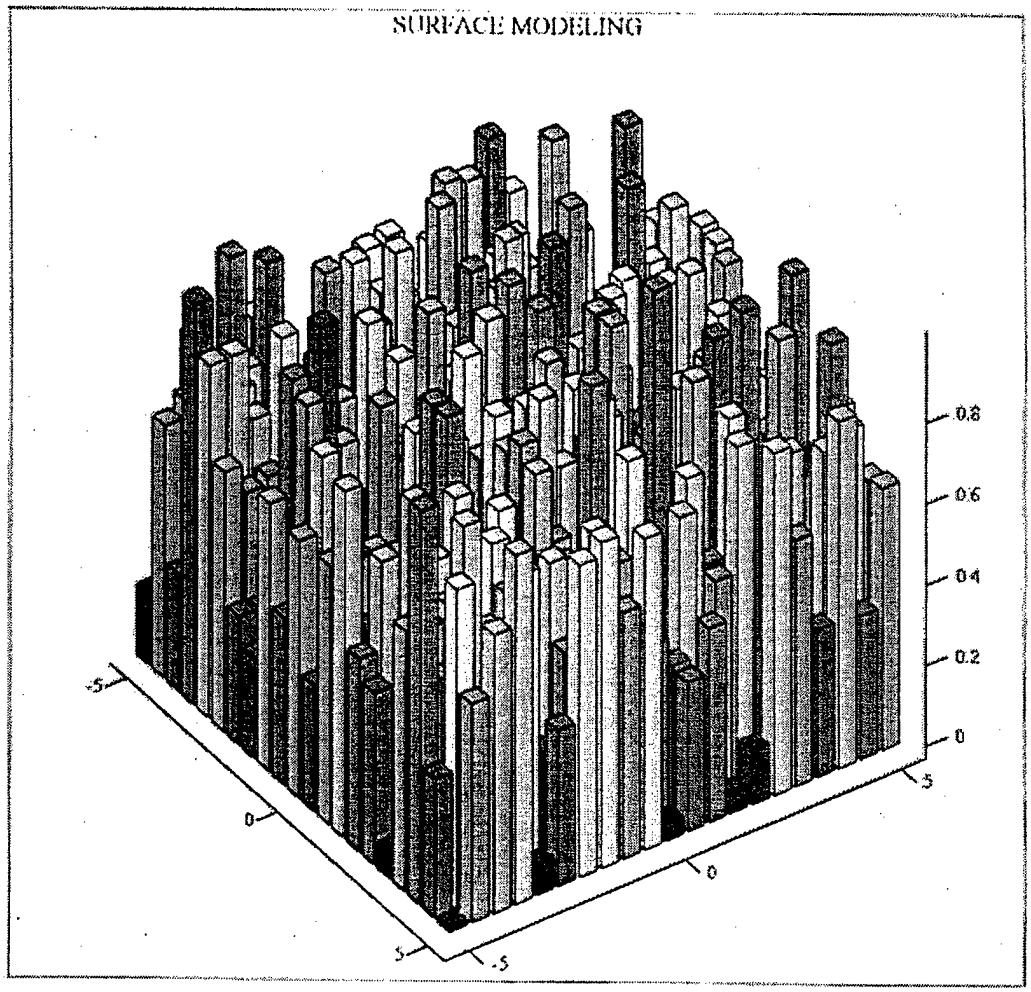

I

Fig.1

$N := 20 \quad i := 1..20 \quad j := 1..20$

$f(x,y) := |\mathrm{rnd}(1)|$

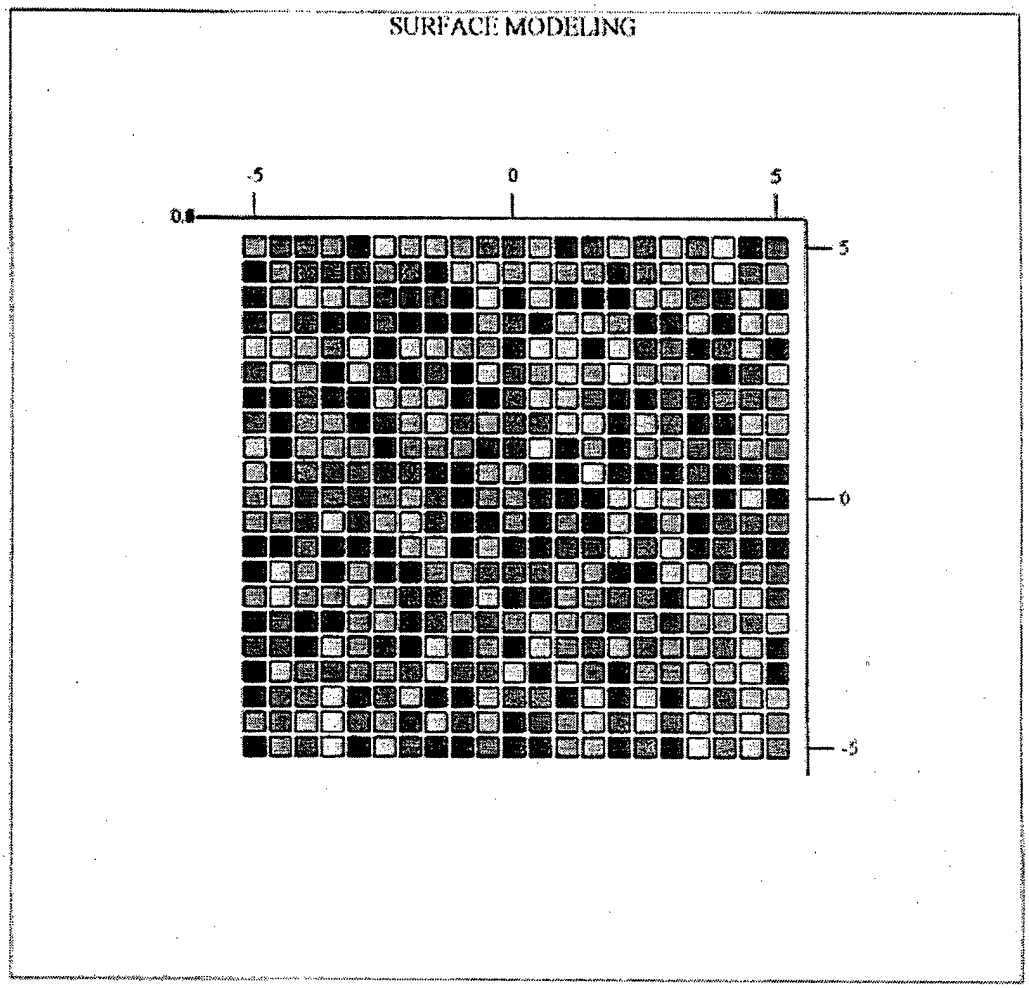

f

Fig.2

ELEMENTARY CELL

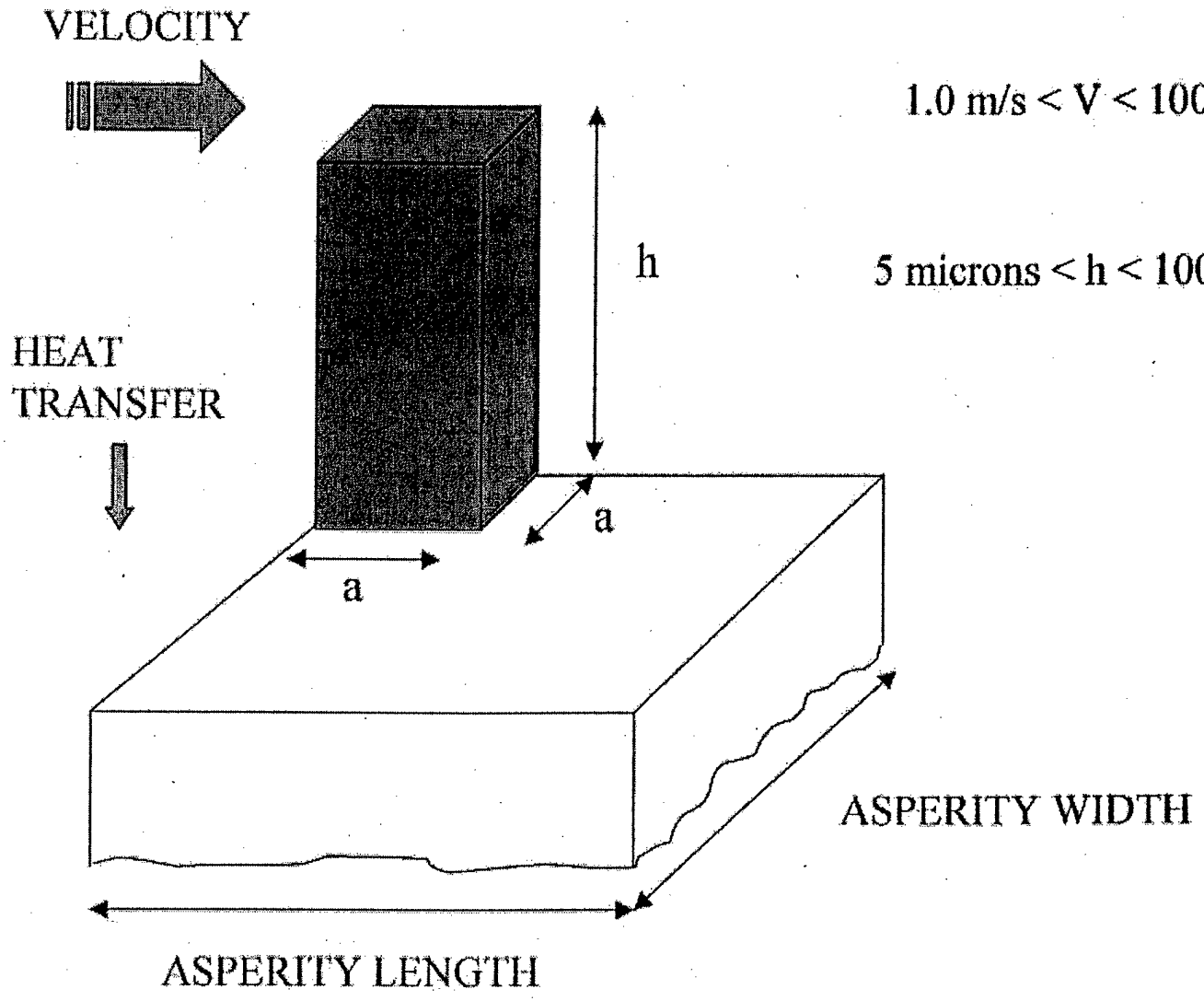

Fig.3

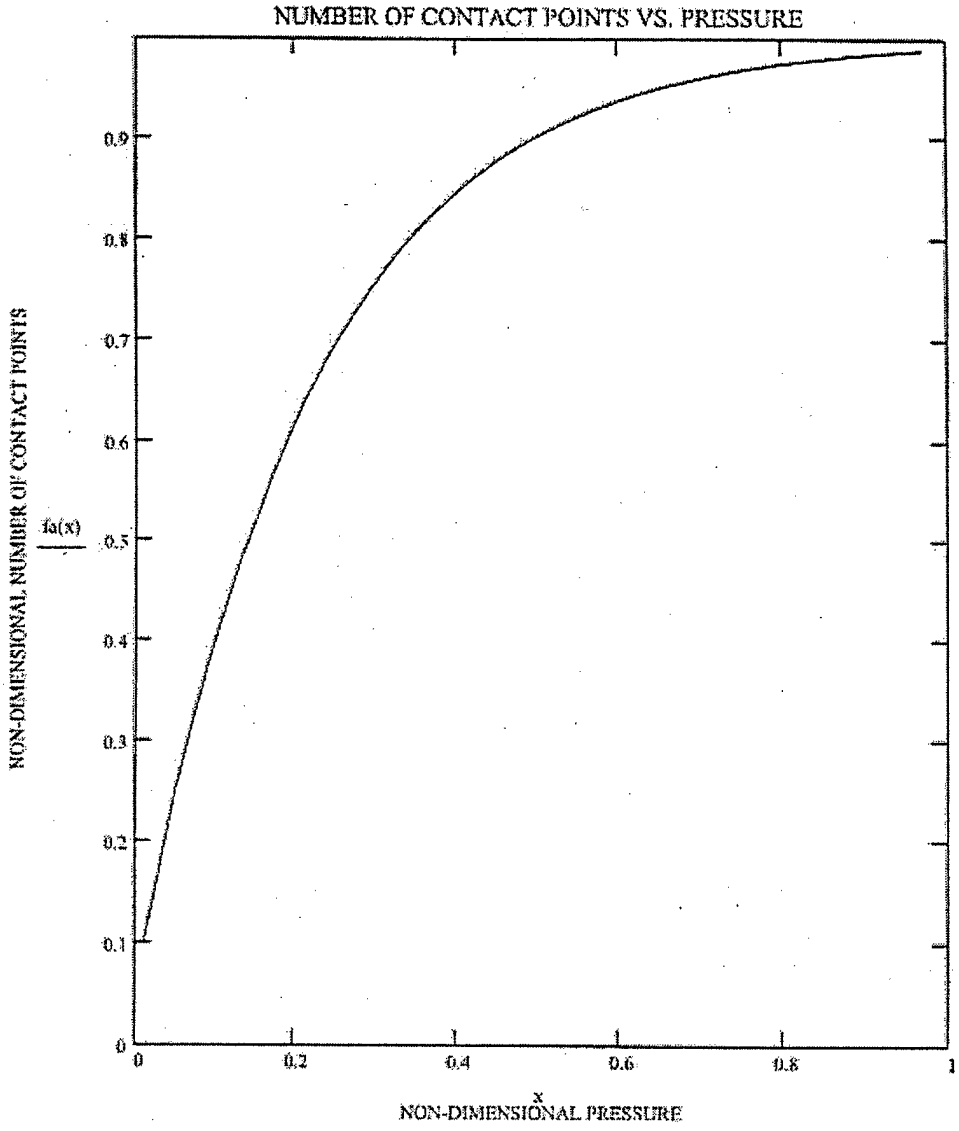
NUMBER OF CONTACT POINTS VS. PRESSURE
NON-DIMENSIONAL NUMBER OF CONTACT POINTS
$\frac{Na(x)}{N}$
0
0.1
0.2
0.3
0.4
0.5
0.6
0.7
0.8
0.9
0
0.2
0.4
0.6
0.8
1
x
NON-DIMENSIONAL PRESSURE

Fig.4

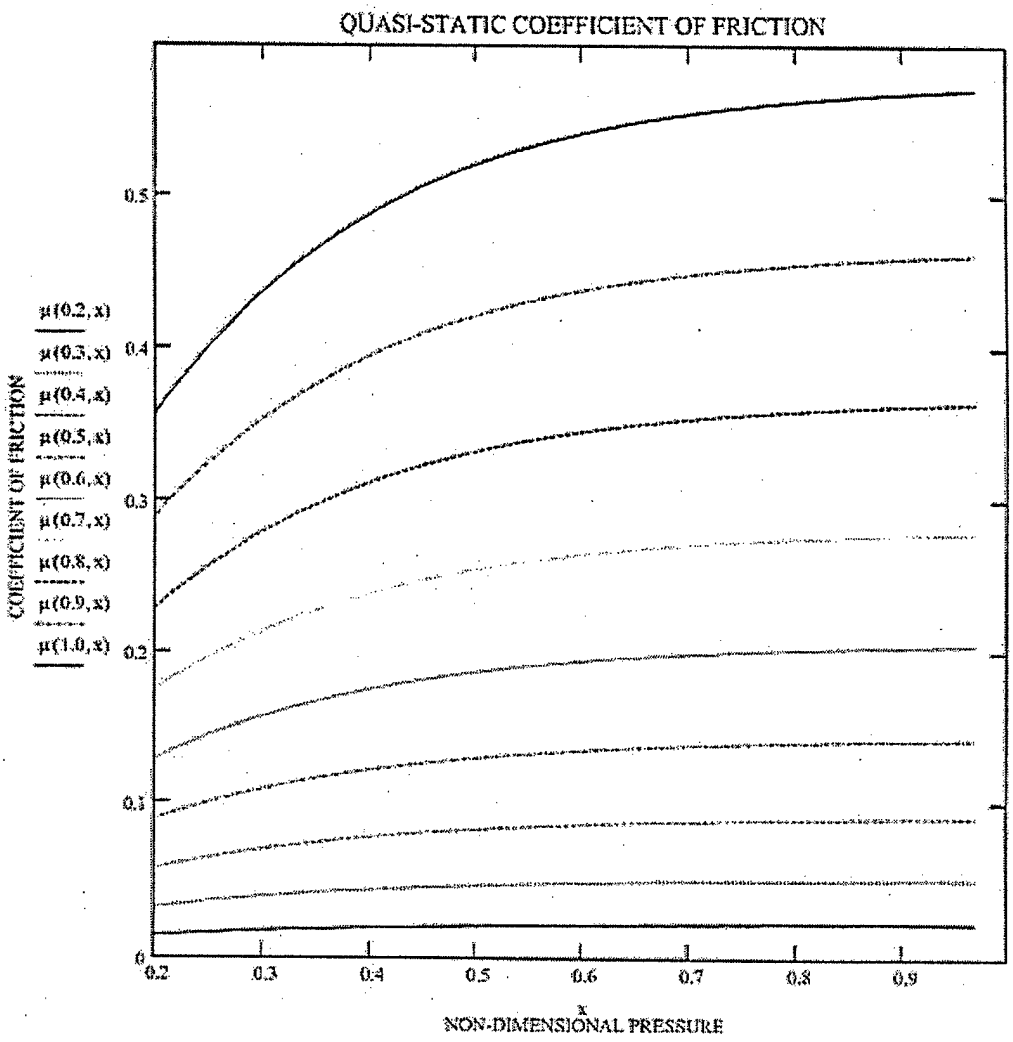
QUASI-STATIC COEFFICIENT OF FRICTION
COEFFICIENT OF FRICTION
μ(0.2, x)
μ(0.3, x)
μ(0.4, x)
μ(0.5, x)
μ(0.6, x)
μ(0.7, x)
μ(0.8, x)
μ(0.9, x)
μ(1.0, x)
0.5
0.4
0.3
0.2
0.1
0
0.2
0.3
0.4
0.5
0.6
0.7
0.8
0.9
x
NON-DIMENSIONAL PRESSURE

Fig.5

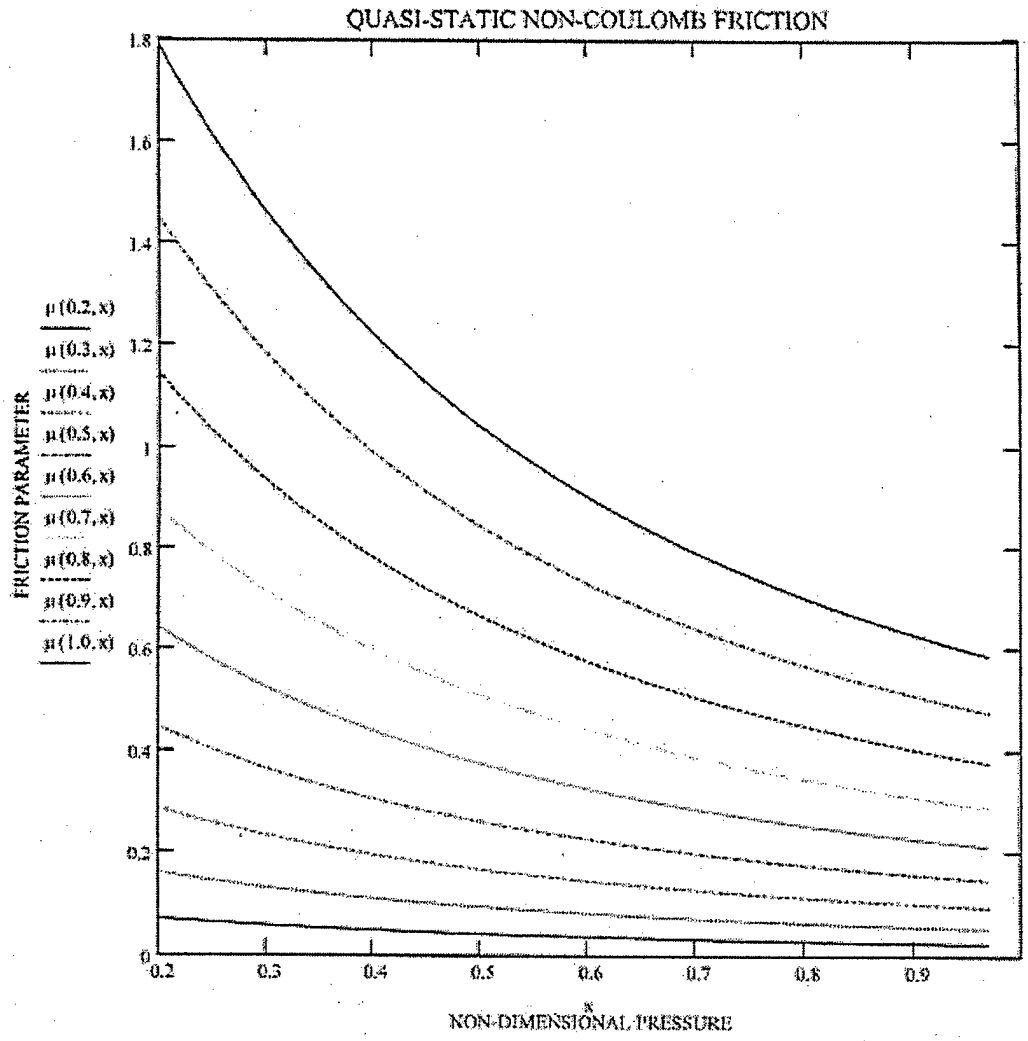
QUASI-STATIC NON-COULOMB FRICTION
FRICTION PARAMETER
NON-DIMENSIONAL PRESSURE
x
μ(0.2, x)
μ(0.3, x)
μ(0.4, x)
μ(0.5, x)
μ(0.6, x)
μ(0.7, x)
μ(0.8, x)
μ(0.9, x)
μ(1.0, x)
0
0.2
0.4
0.6
0.8
1
1.2
1.4
1.6
1.8
0.2
0.3
0.4
0.5
0.6
0.7
0.8
0.9

Fig.6

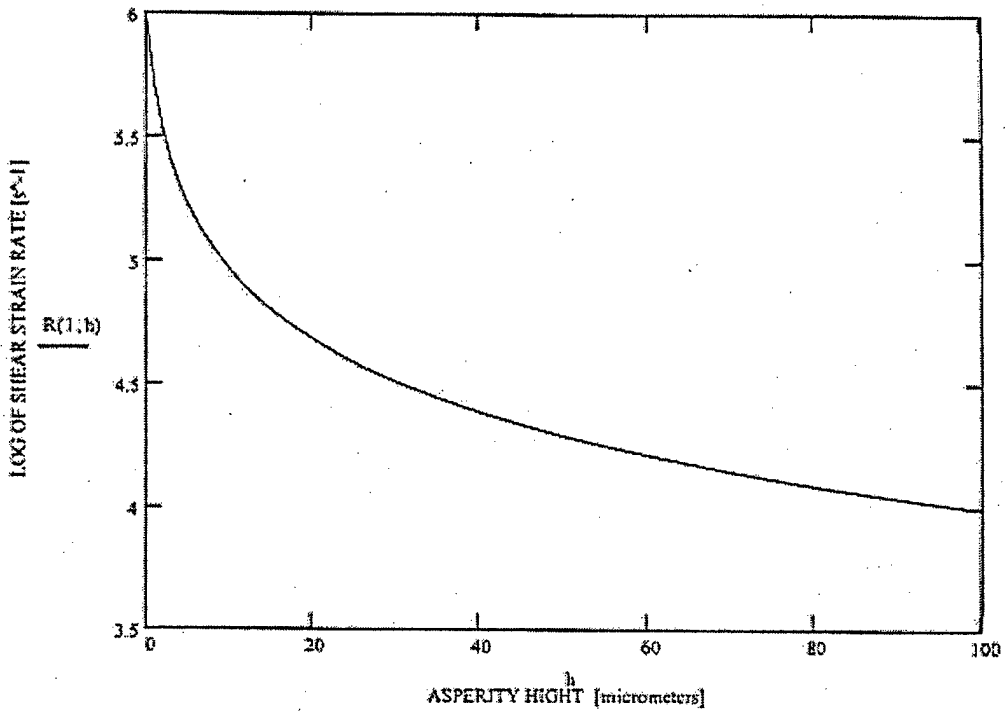
LOG OF SHEAR STRAIN RATE [s^-1]
R(1,h)
6
5.5
5
4.5
4
3.5
0
20
40
60
80
100
h
ASPERITY HIGHT [micrometers]

Fig.7

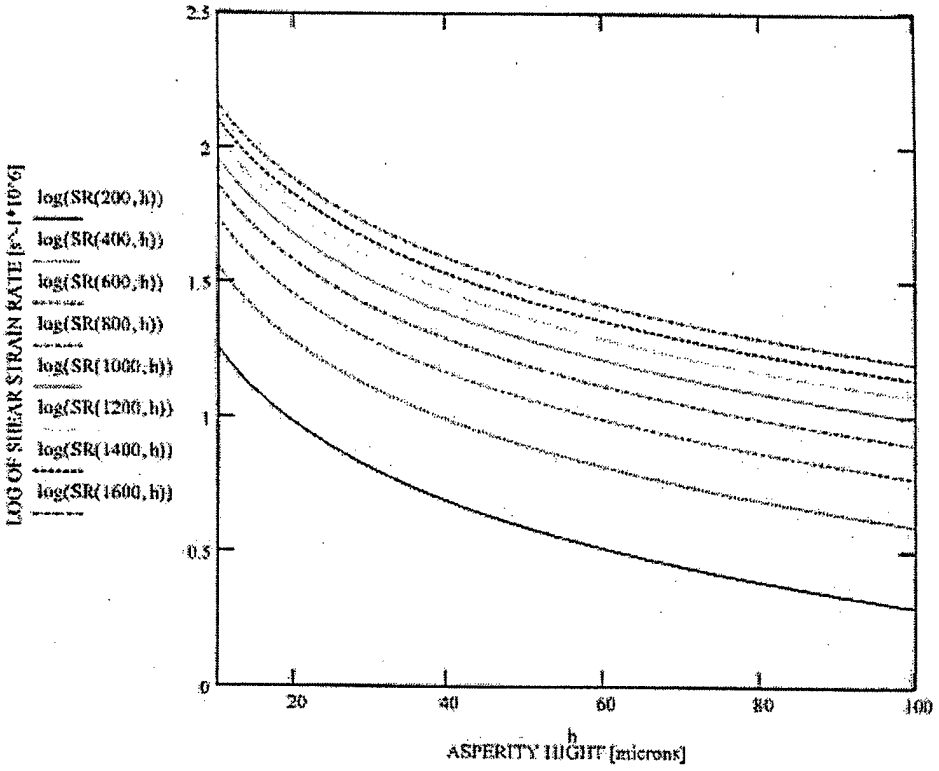
LOG OF SHEAR STRAIN RATE [s^-1*10^6]
log(SR(200,h))
log(SR(400,h))
log(SR(600,h))
log(SR(800,h))
log(SR(1000,h))
log(SR(1200,h))
log(SR(1400,h))
log(SR(1600,h))
2.5
2
1.5
1
0.5
0
20
40
60
80
100
h
ASPERITY HEIGHT [microns]

Fig.8

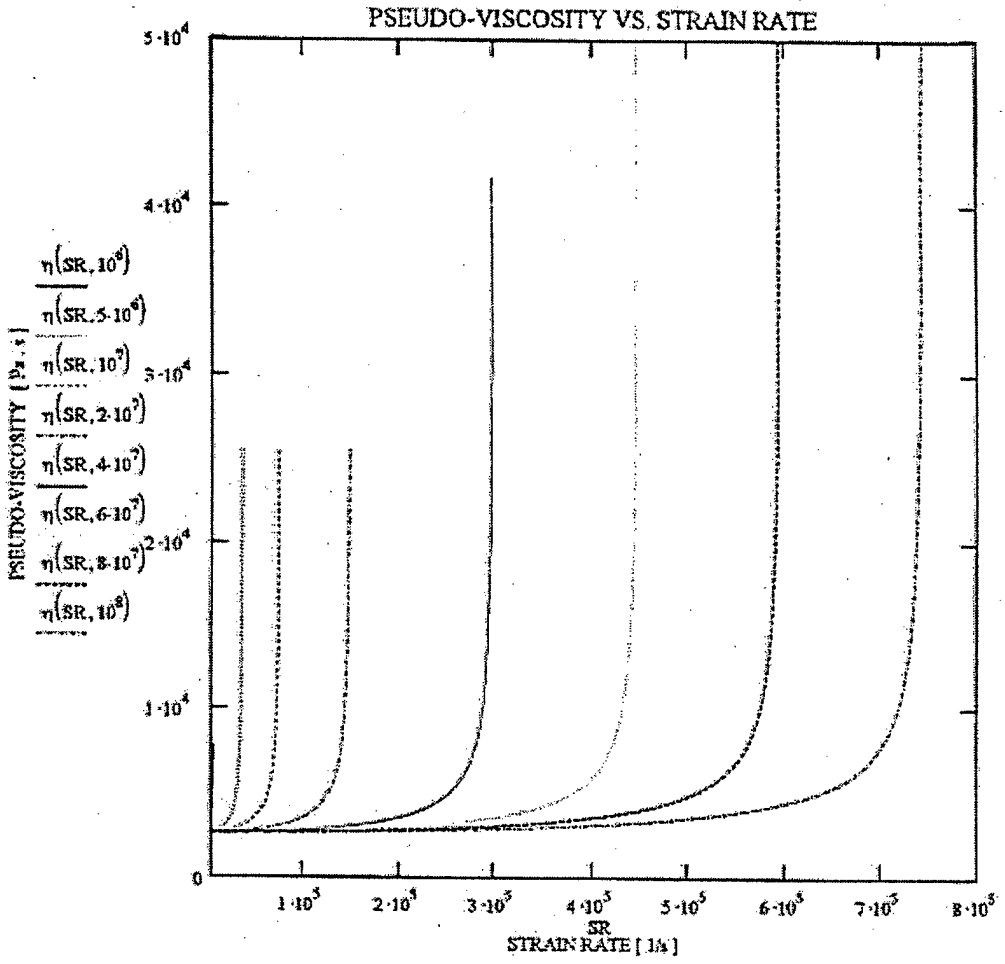
PSEUDO-VISCOSITY VS. STRAIN RATE
PSEUDO-VISCOSITY [Pa . s]
η(SR, 10^6)
η(SR, 5·10^6)
η(SR, 10^7)
η(SR, 2·10^7)
η(SR, 4·10^7)
η(SR, 6·10^7)
η(SR, 8·10^7)
η(SR, 10^8)
5·10^4
4·10^4
3·10^4
2·10^4
1·10^4
0
1·10^5
2·10^5
3·10^5
4·10^5
5·10^5
6·10^5
7·10^5
8·10^5
SR
STRAIN RATE [1/s]

Fig.9

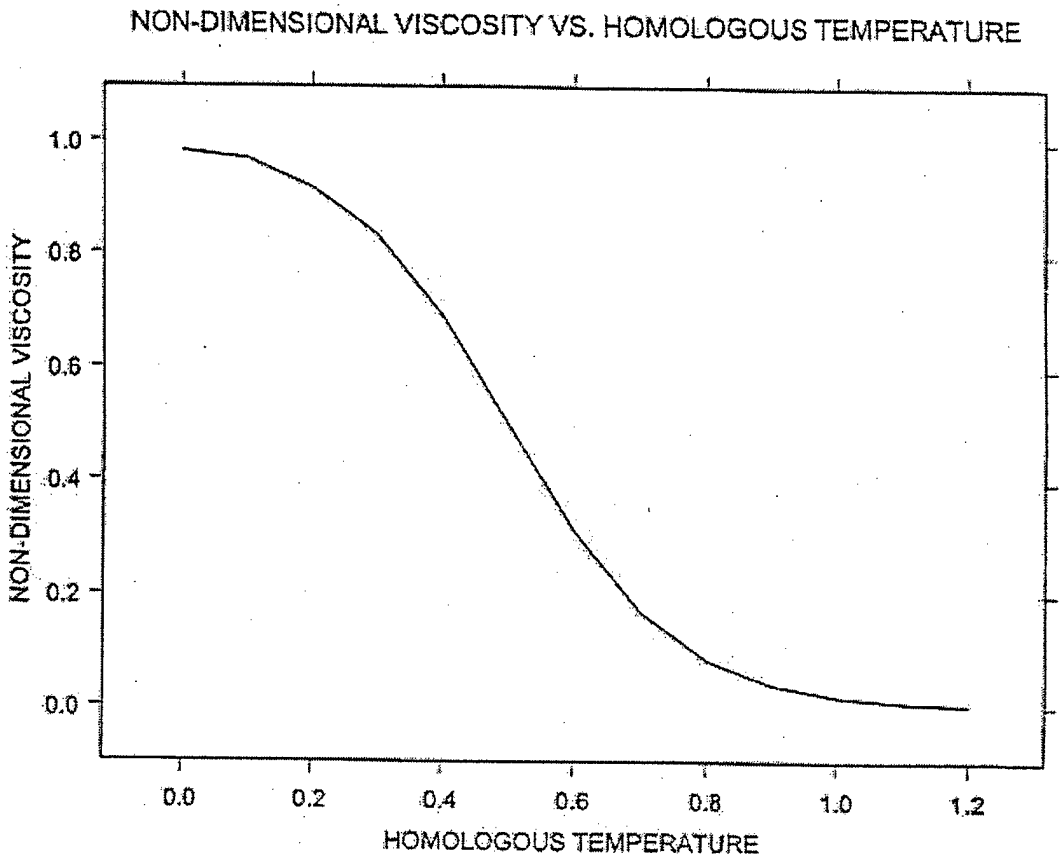
NON-DIMENSIONAL VISCOSITY VS. HOMOLOGOUS TEMPERATURE
NON-DIMENSIONAL VISCOSITY
1.0
0.8
0.6
0.4
0.2
0.0
0.0
0.2
0.4
0.6
0.8
1.0
1.2
HOMOLOGOUS TEMPERATURE

Fig.10

ELEMENTARY CELL FAILURE

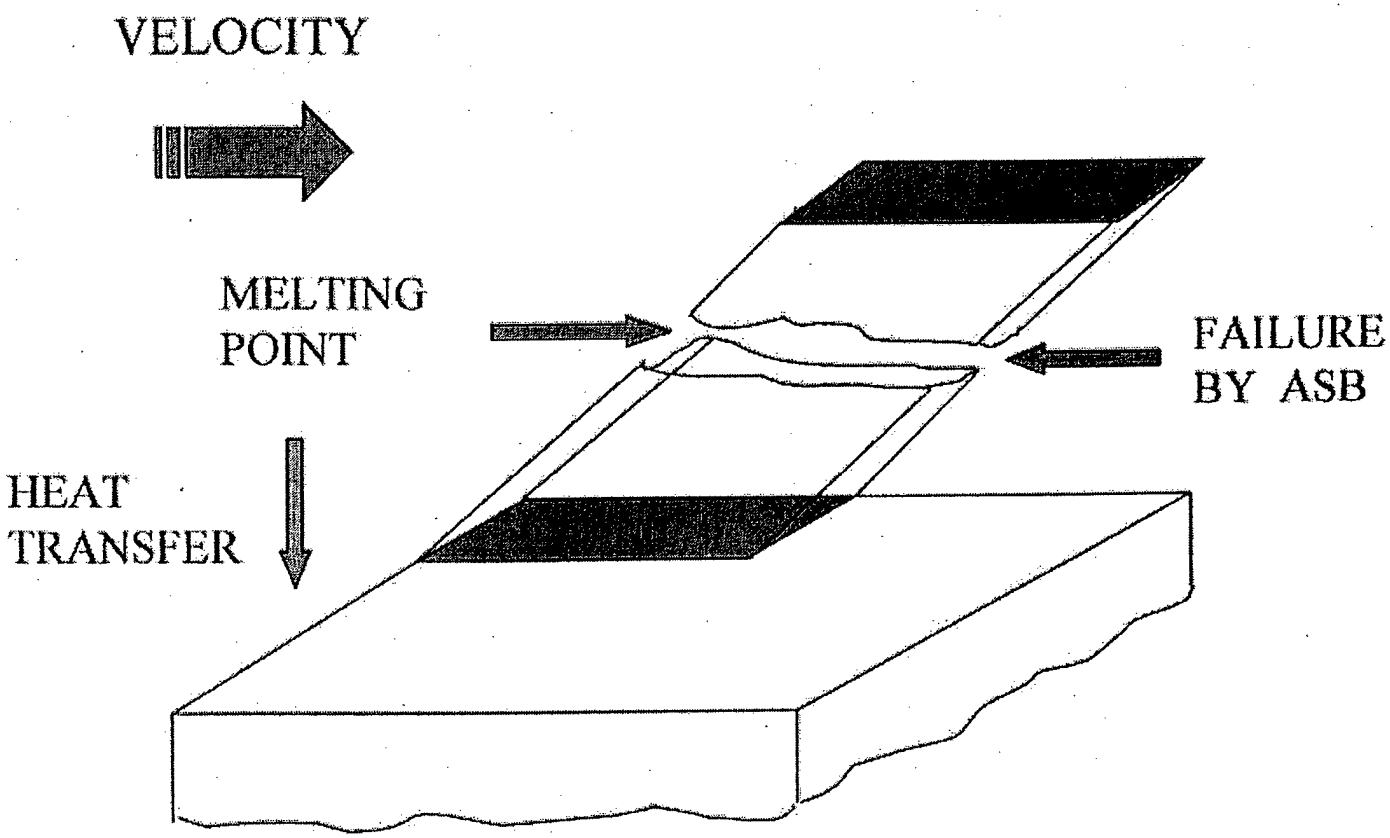

Fig.11

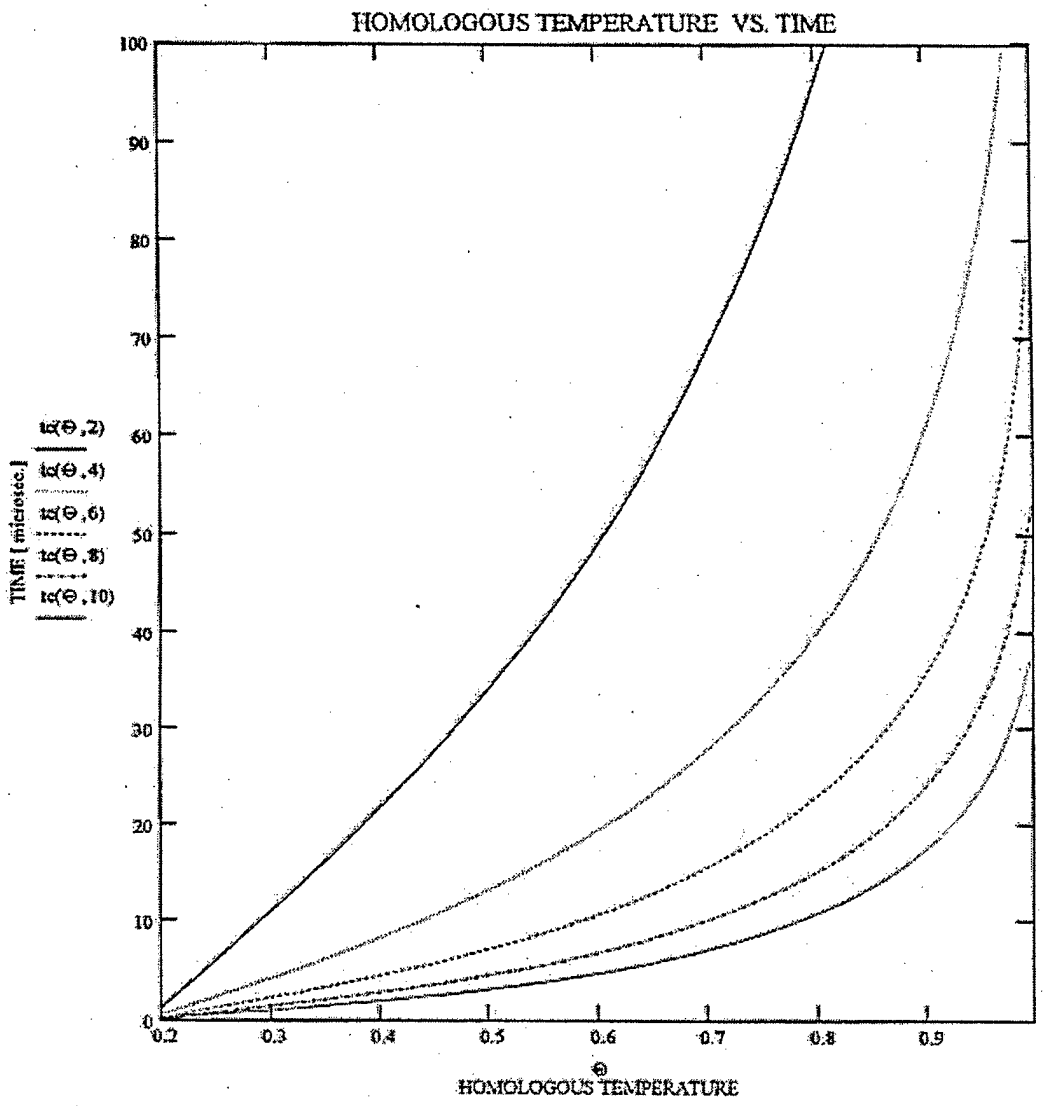
HOMOLOGOUS TEMPERATURE VS. TIME
TIME [microsec.]
tc(Θ,2)
tc(Θ,4)
tc(Θ,6)
tc(Θ,8)
tc(Θ,10)
100
90
80
70
60
50
40
30
20
10
0
0.2
0.3
0.4
0.5
0.6
0.7
0.8
0.9
Θ
HOMOLOGOUS TEMPERATURE

Fig.12a

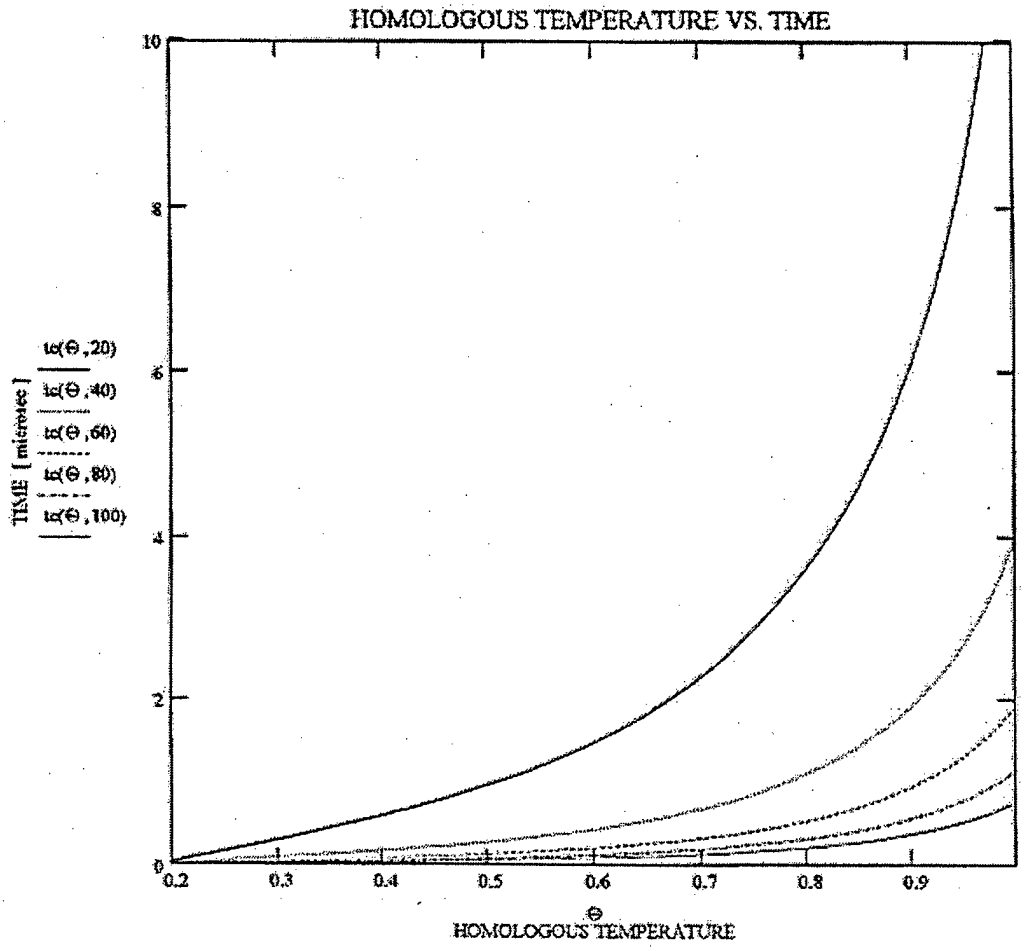
HOMOLOGOUS TEMPERATURE VS. TIME
TIME [microsec]
t(Θ,20)
t(Θ,40)
t(Θ,60)
t(Θ,80)
t(Θ,100)
10
8
6
4
2
0
0.2
0.3
0.4
0.5
0.6
0.7
0.8
0.9
Θ
HOMOLOGOUS TEMPERATURE

Fig.12b

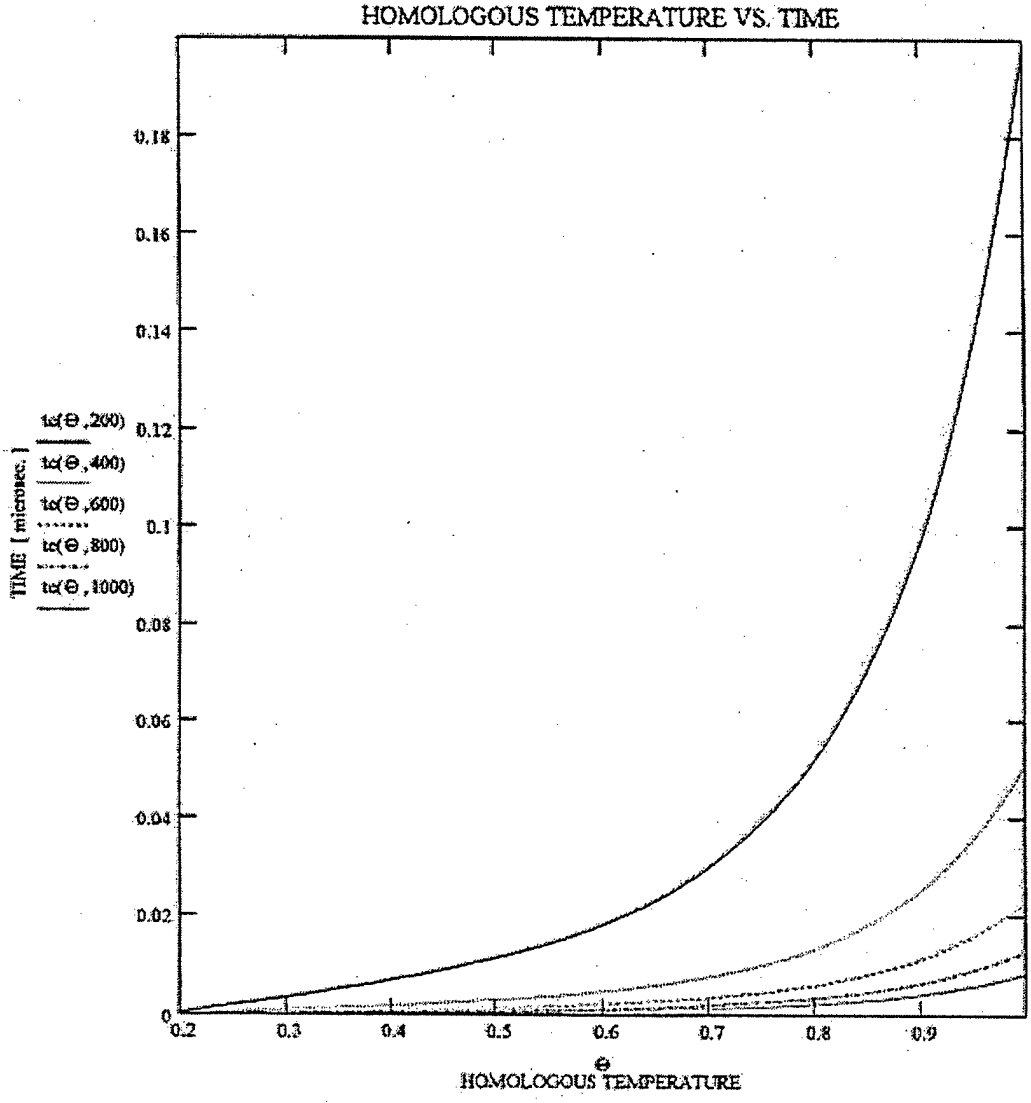
HOMOLOGOUS TEMPERATURE VS. TIME
TIME [microsec.]
tc(Θ,200)
tc(Θ,400)
tc(Θ,600)
tc(Θ,800)
tc(Θ,1000)
0.18
0.16
0.14
0.12
0.1
0.08
0.06
0.04
0.02
0
0.2
0.3
0.4
0.5
0.6
0.7
0.8
0.9
Θ
HOMOLOGOUS TEMPERATURE

Fig.12c

$$tc(\Theta, V) := \int_{\Theta o}^{\Theta} f(\Theta, V)\, d\Theta$$

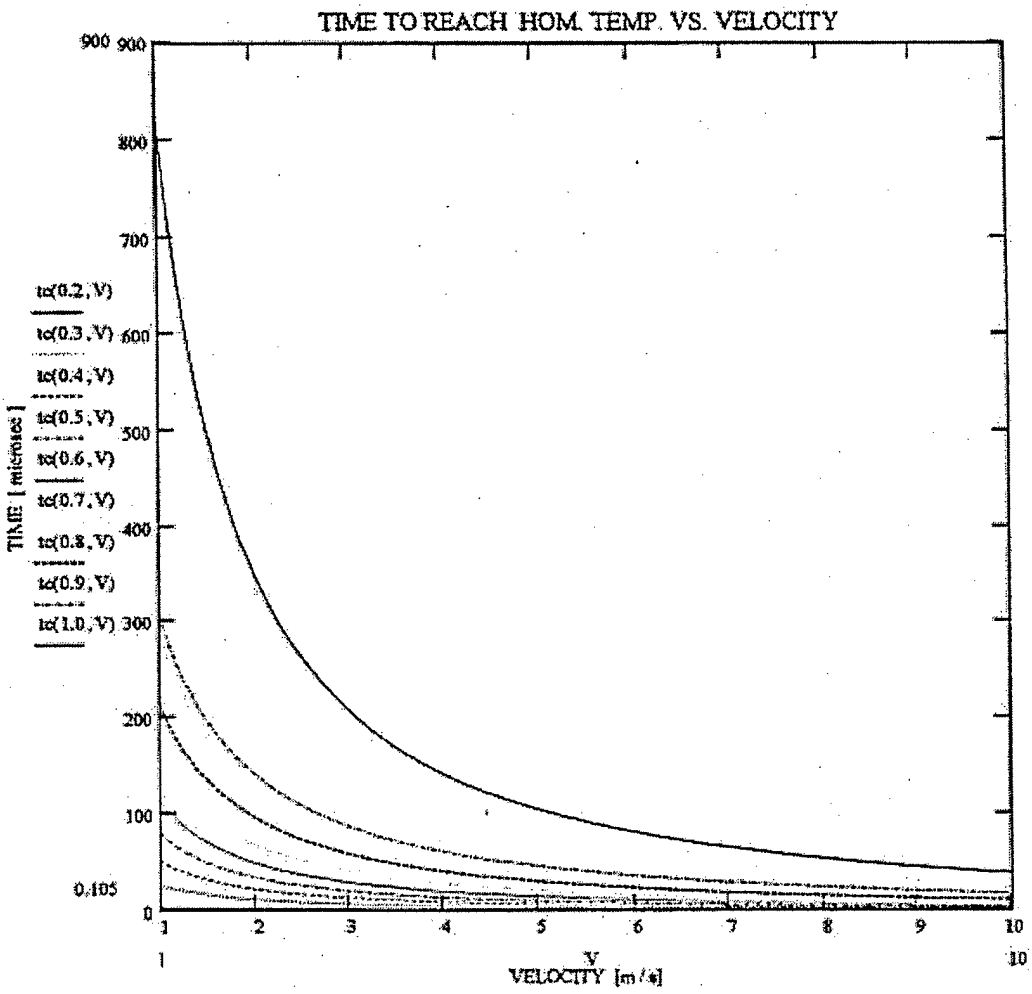

Fig.13a

$V := 10, 11 .. 100$

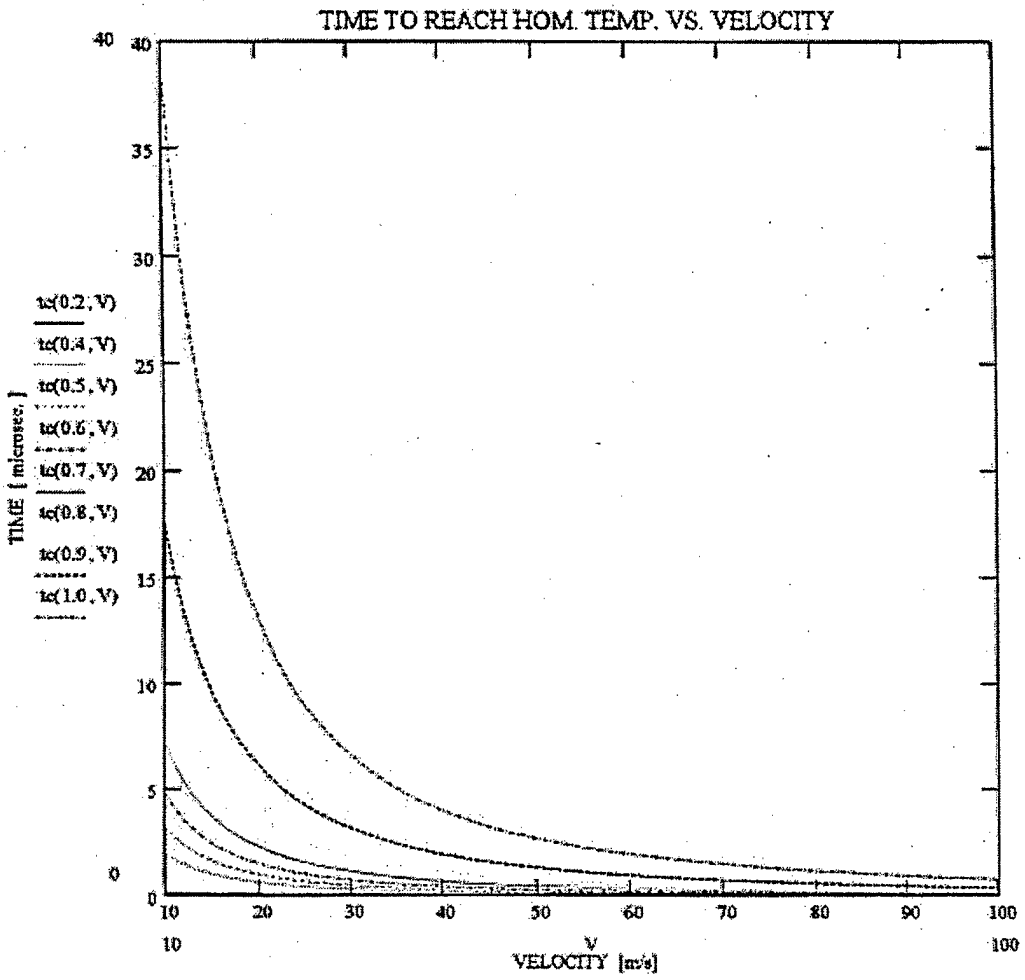

Fig.13b

V := 100, 110 .. 1000

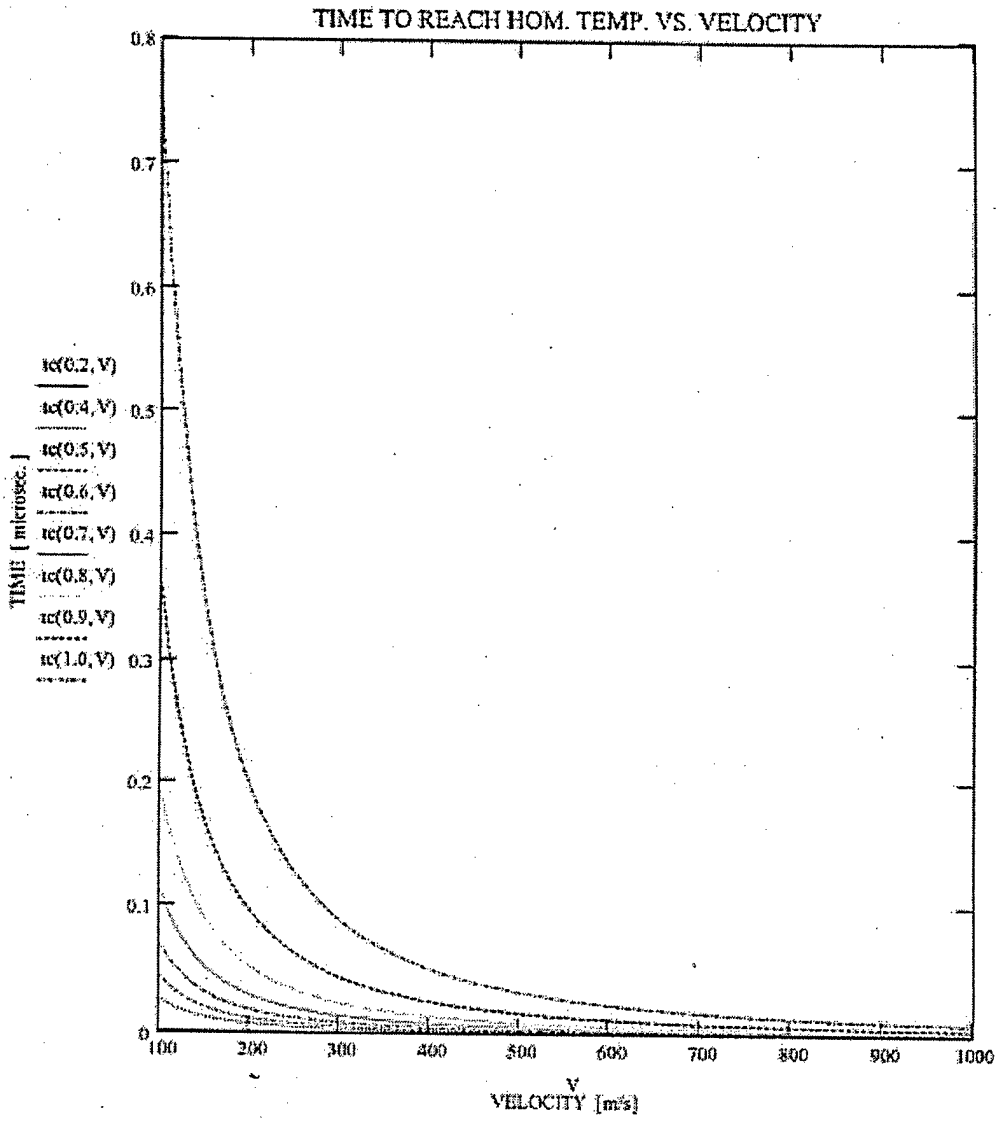

Fig.13c

$V := 1, 1.2 .. 10$

$\Gamma c := 2$

$$ft(V) := \Gamma c \cdot \frac{h}{V}$$

$$\frac{\int_{\Theta w}^{1} \frac{h \cdot 10^6}{Cl \cdot V \cdot \tau o \cdot \left(1 - \Theta^2 + \eta o \cdot V \cdot \frac{fn(\Theta)}{2 \cdot \tau o \cdot h}\right)} d\Theta}{ft(V) \cdot 10^6}$$

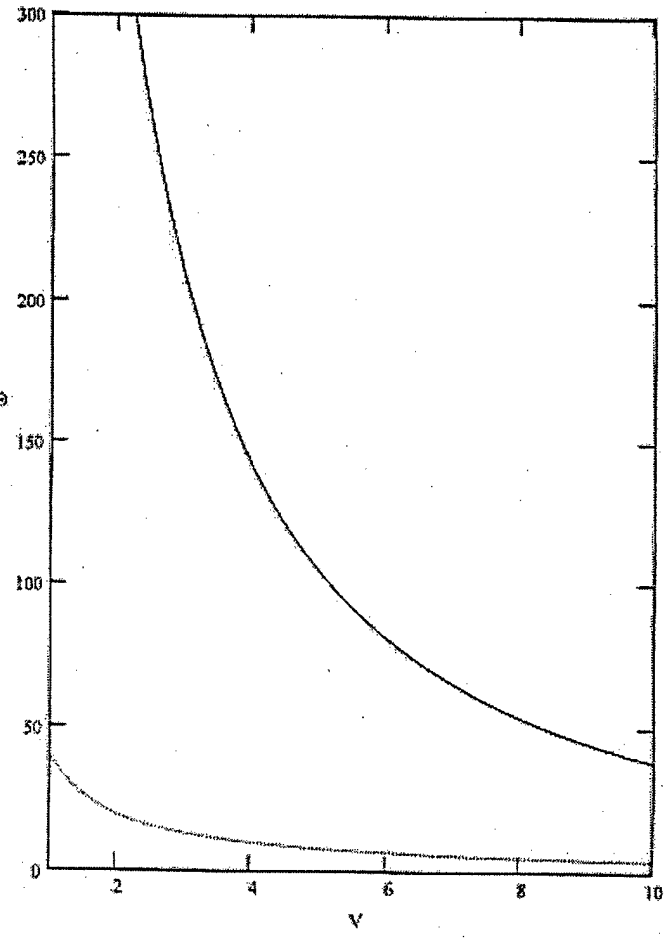

Fig.14a

$V := 10, 12 .. 100$

$\Gamma c := 2$

$$ft(V) := \Gamma c \cdot \frac{h}{V}$$

$$\frac{\int_{\Theta o}^{1} \frac{h \cdot 10^{6}}{C1 \cdot V \cdot \tau o \cdot \left(1 - \Theta^{2} + \eta o \cdot V \cdot \frac{fi(\Theta)}{2 \cdot \tau o \cdot h}\right)} d\Theta}{ft(V) \cdot 10^{6}}$$

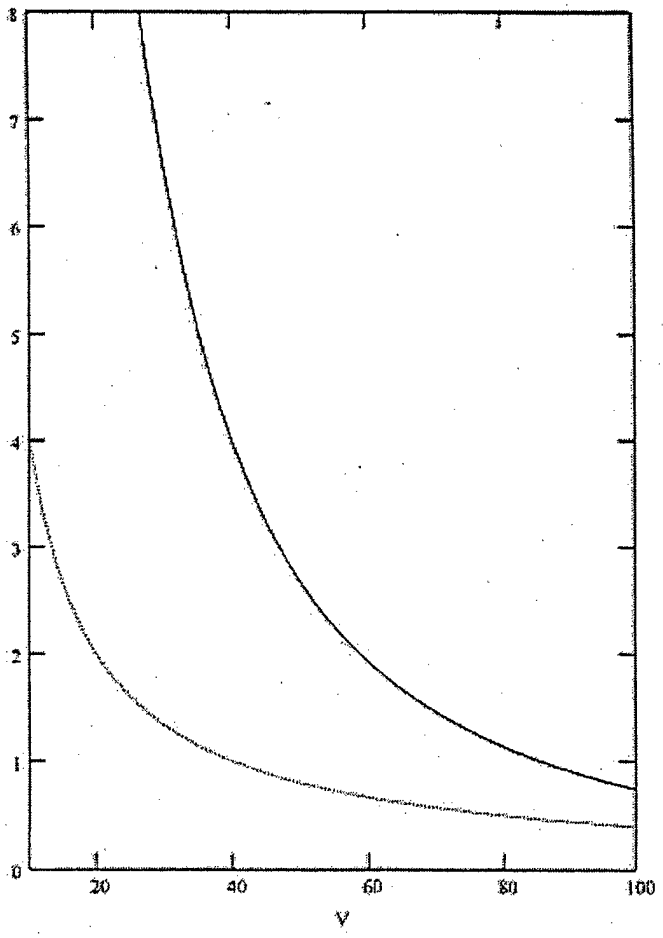

Fig.14b

$V := 100, 120 .. 1000$

$\Gamma c := 2$

$$ft(V) := \Gamma c \cdot \frac{h}{V}$$

$$\frac{\int_{\Theta_0}^{1} \frac{h \cdot 10^6}{C1 \cdot V \cdot \pi \cdot \left(1 - \Theta^2 + \eta o \cdot V \cdot \frac{\tilde{n}_1(\Theta)}{2 \cdot \pi o \cdot h}\right)} d\Theta}{ft(V) \cdot 10^6}$$

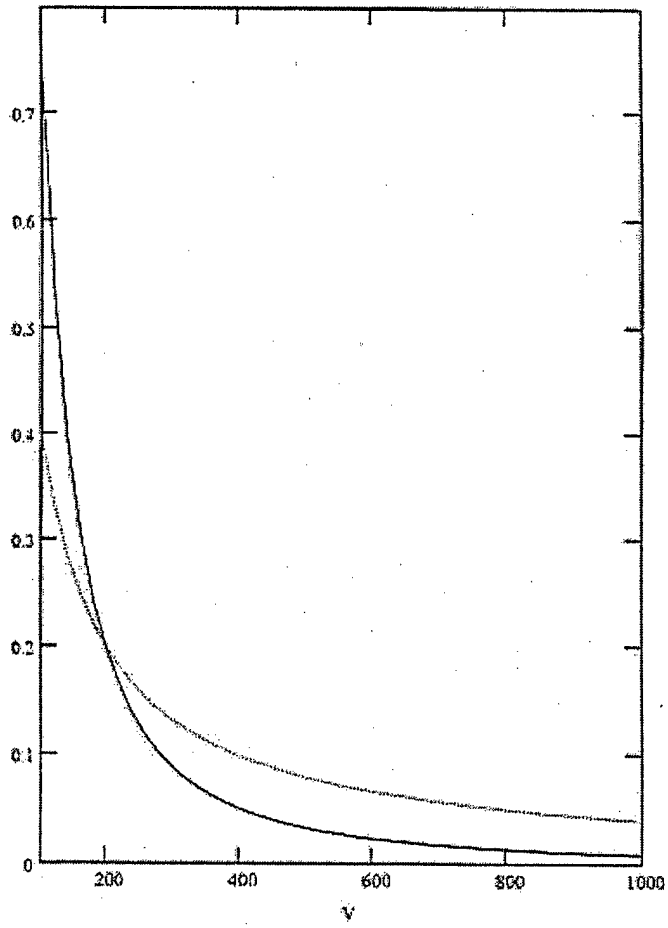

Fig.14c

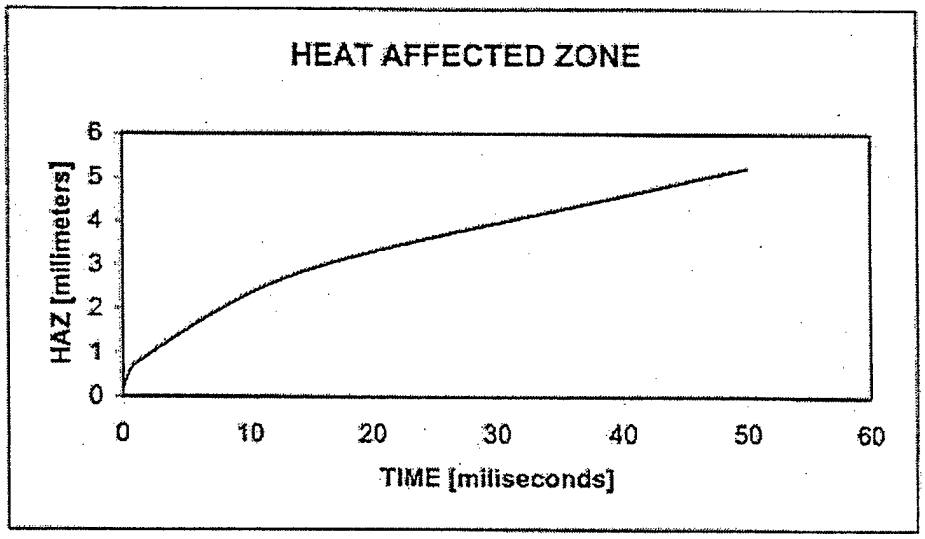
HEAT AFFECTED ZONE
HAZ [millimeters]
0
1
2
3
4
5
6
0
10
20
30
40
50
60
TIME [miliseconds]

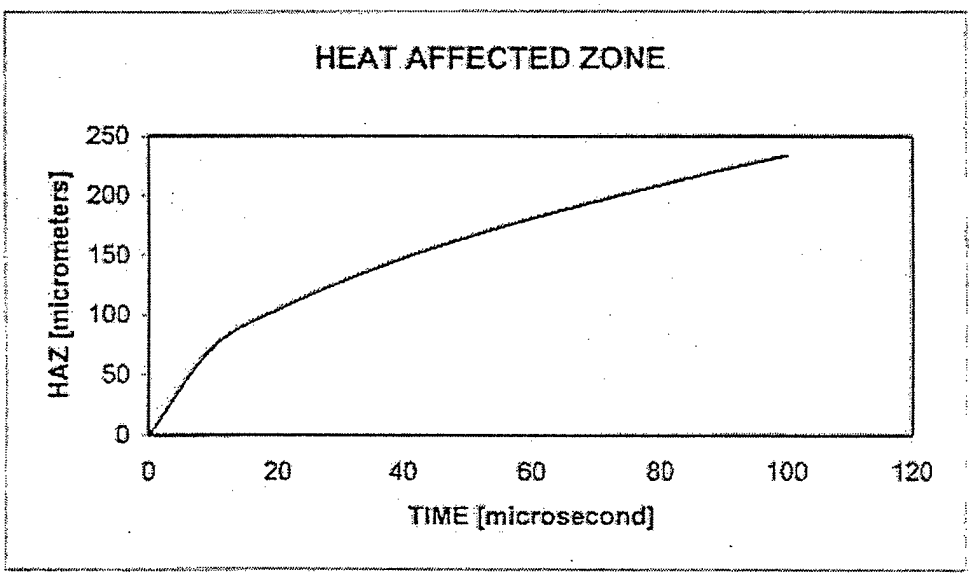
HEAT AFFECTED ZONE
HAZ [micrometers]
0
50
100
150
200
250
0
20
40
60
80
100
120
TIME [microsecond]

Fig.15

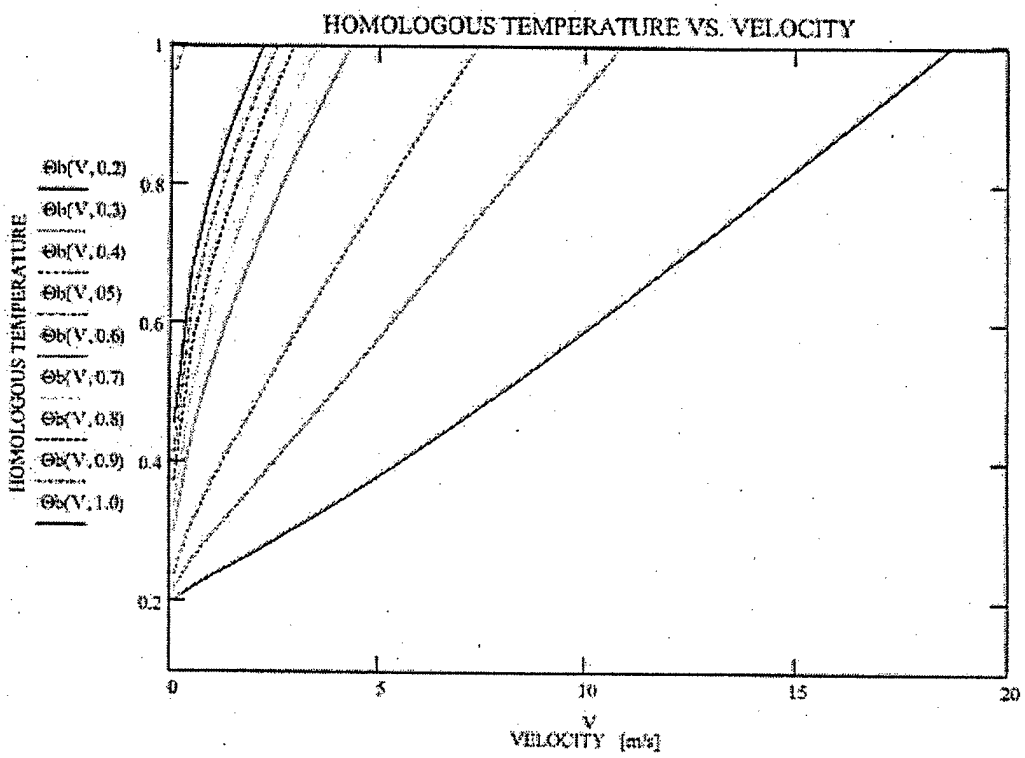
HOMOLOGOUS TEMPERATURE VS. VELOCITY
HOMOLOGOUS TEMPERATURE
Θb(V, 0.2)
Θb(V, 0.3)
Θb(V, 0.4)
Θb(V, 05)
Θb(V, 0.6)
Θb(V, 0.7)
Θb(V, 0.8)
Θb(V, 0.9)
Θb(V, 1.0)
1
0.8
0.6
0.4
0.2
0
5
10
15
20
V
VELOCITY [m/s]

Fig.16

$V := 0, 0.01 .. 1$

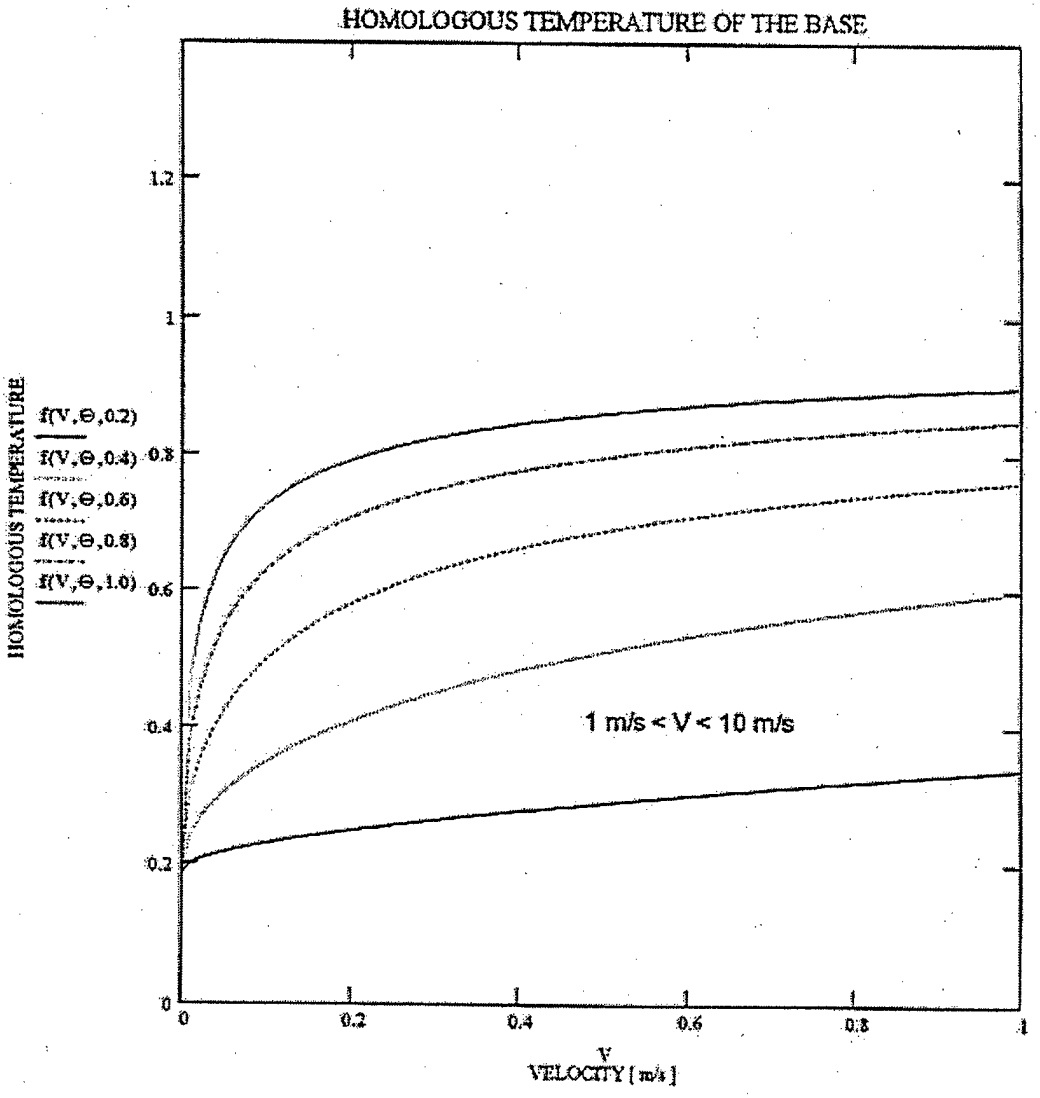

Fig.17a

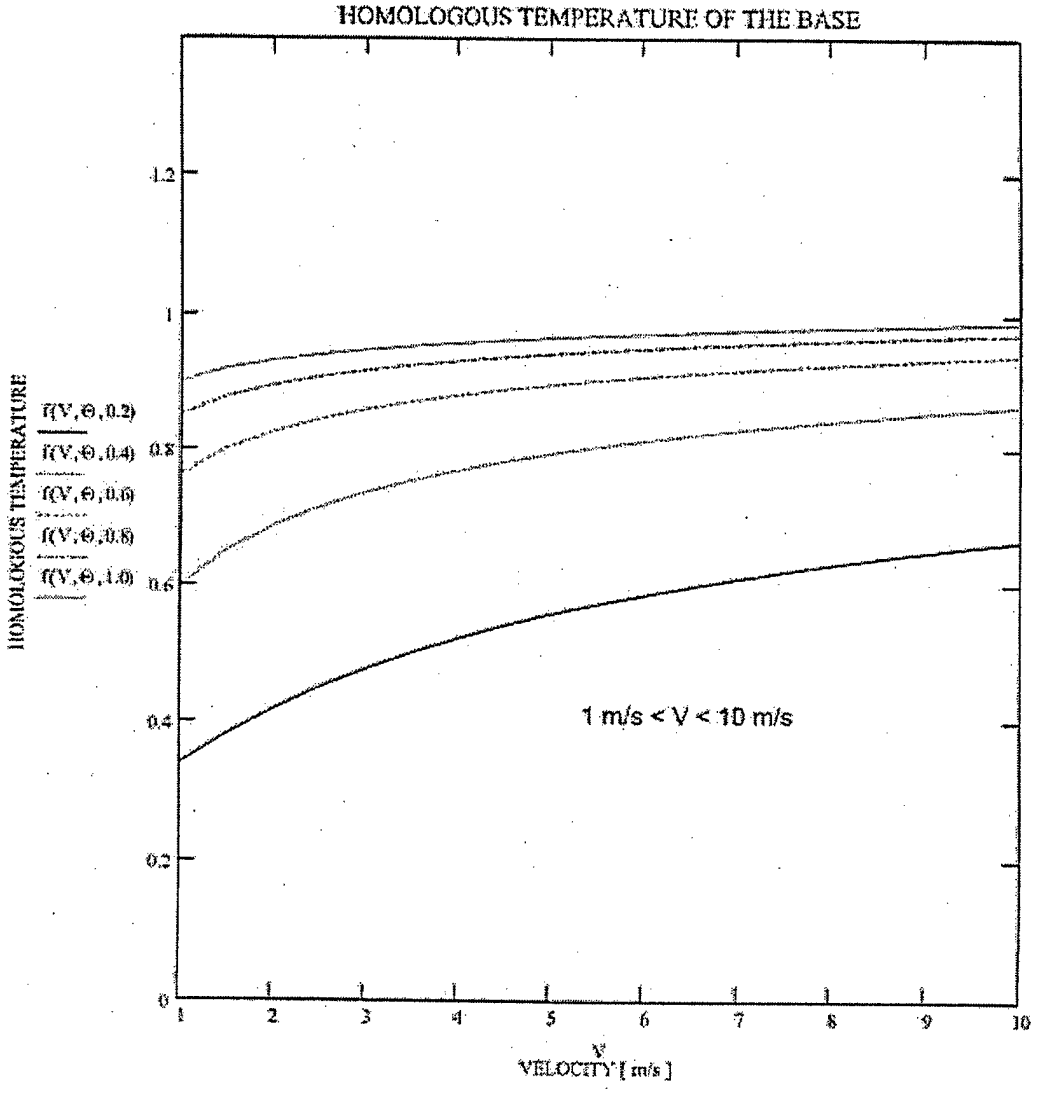
HOMOLOGOUS TEMPERATURE OF THE BASE
HOMOLOGOUS TEMPERATURE
f(V,Θ,0.2)
f(V,Θ,0.4)
f(V,Θ,0.6)
f(V,Θ,0.8)
f(V,Θ,1.0)
1.2
1
0.8
0.6
0.4
0.2
0
1
2
3
4
5
6
7
8
9
10
1 m/s < V < 10 m/s
V
VELOCITY [m/s]

Fig.17b

V := 10, 15 .. 100

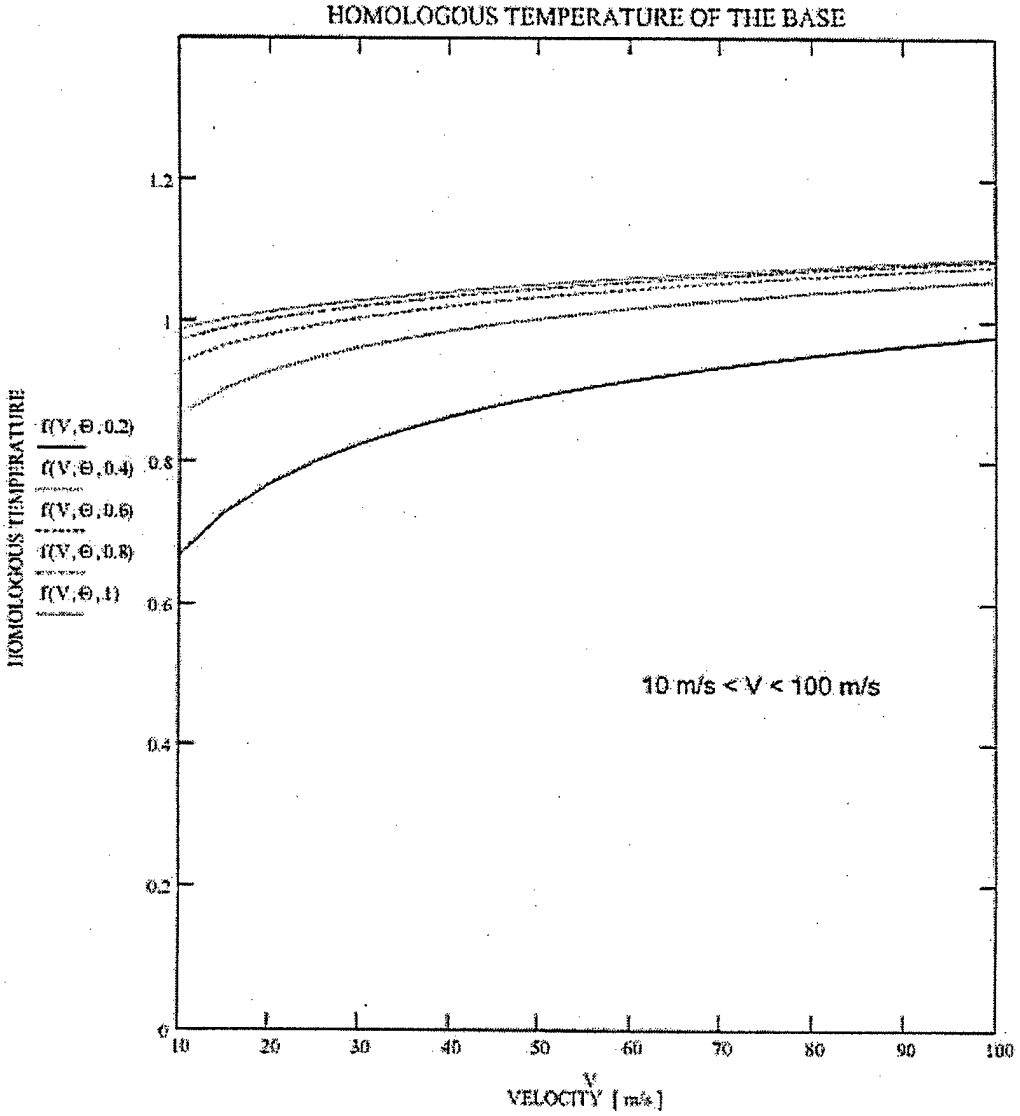

Fig.17c

V := 100, 150.. 1000

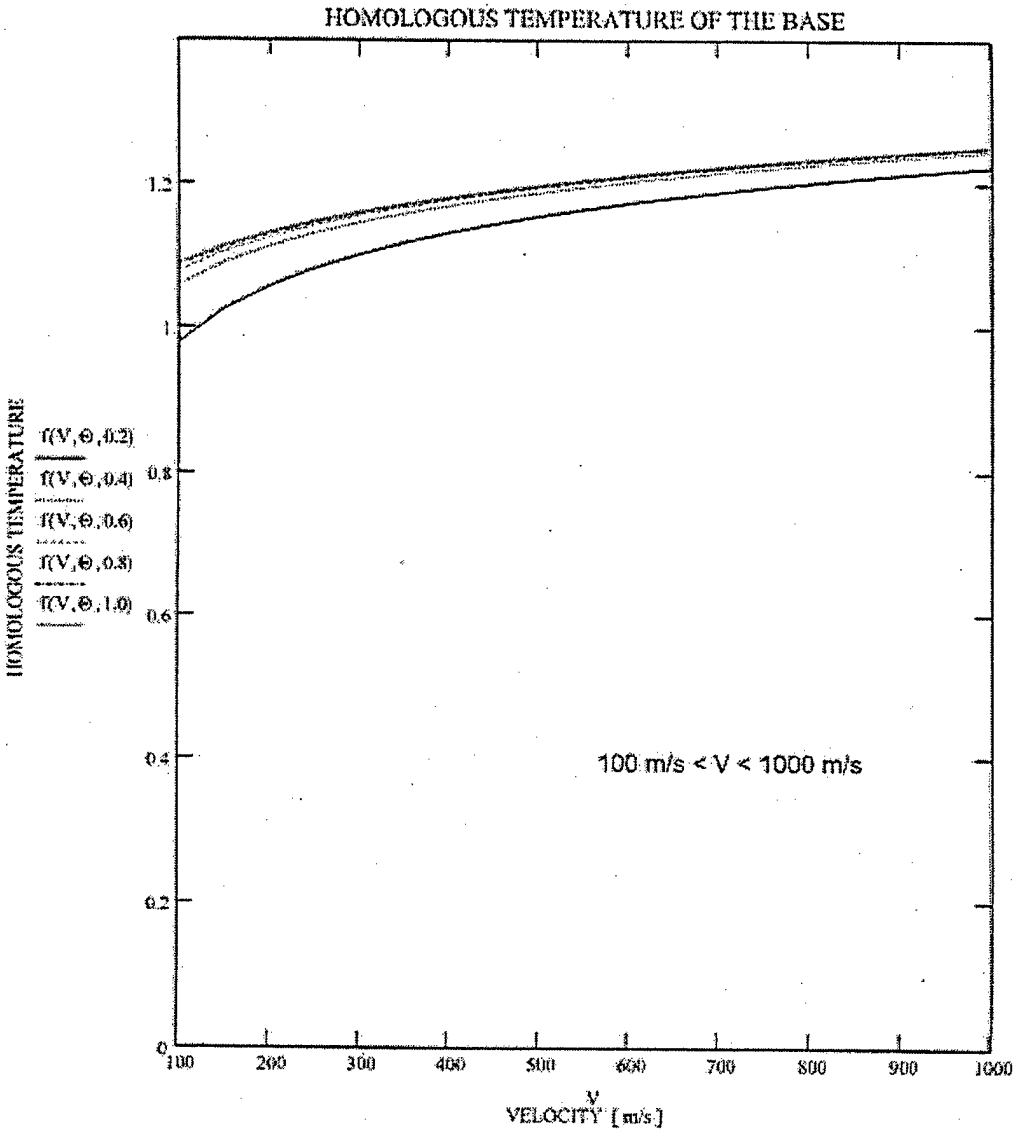

Fig.17d

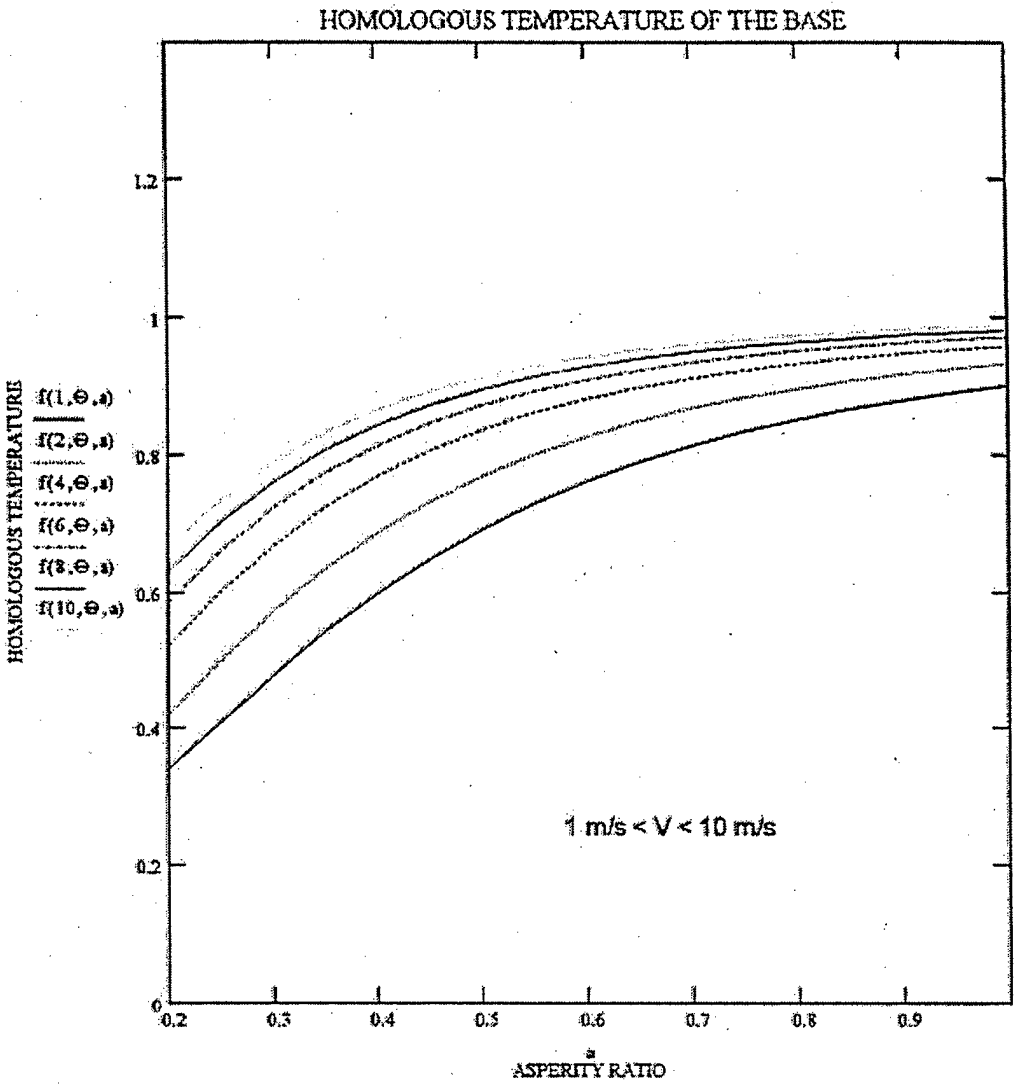
HOMOLOGOUS TEMPERATURE OF THE BASE
HOMOLOGOUS TEMPERATURE
f(1,Θ,a)
f(2,Θ,a)
f(4,Θ,a)
f(6,Θ,a)
f(8,Θ,a)
f(10,Θ,a)
1.2
1
0.8
0.6
0.4
0.2
0
0.2
0.3
0.4
0.5
0.6
0.7
0.8
0.9
a
ASPERITY RATIO
1 m/s < V < 10 m/s

Fig18a

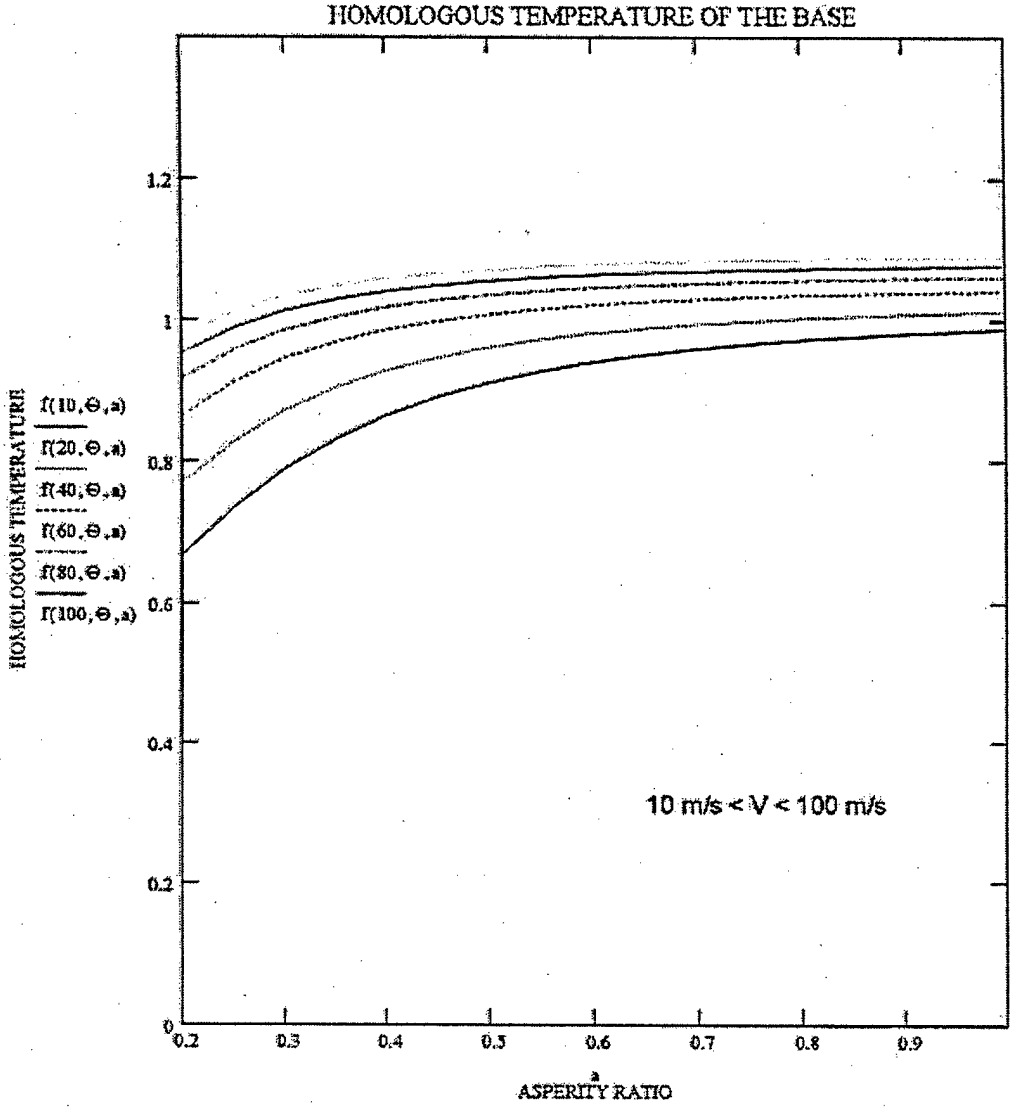
HOMOLOGOUS TEMPERATURE OF THE BASE
HOMOLOGOUS TEMPERATURE
f(10,Θ,a)
f(20,Θ,a)
f(40,Θ,a)
f(60,Θ,a)
f(80,Θ,a)
f(100,Θ,a)
1.2
1
0.8
0.6
0.4
0.2
0
0.2
0.3
0.4
0.5
0.6
0.7
0.8
0.9
a
ASPERITY RATIO
10 m/s < V < 100 m/s

Fig.18b

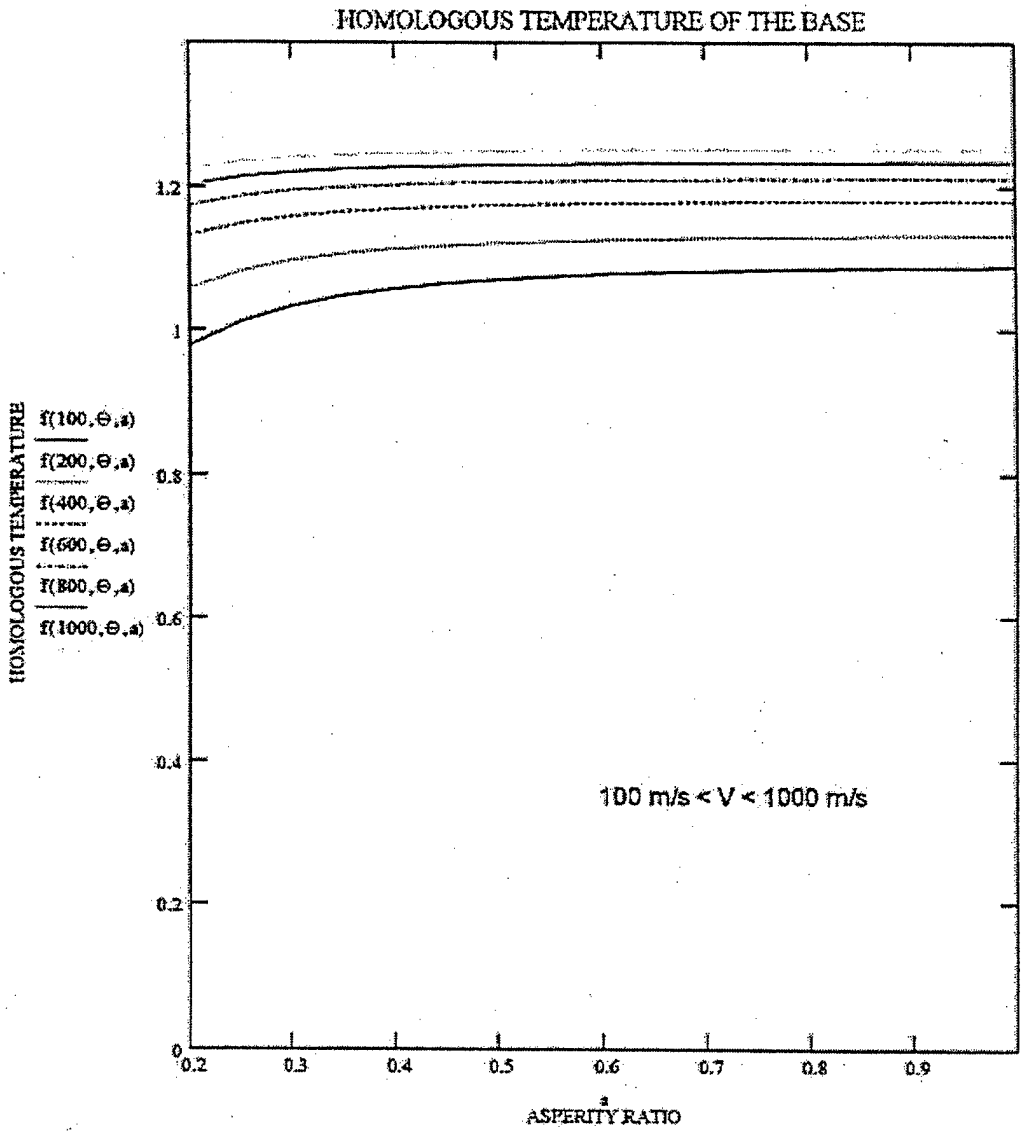
HOMOLOGOUS TEMPERATURE OF THE BASE
HOMOLOGOUS TEMPERATURE
f(100,Θ,a)
f(200,Θ,a)
f(400,Θ,a)
f(600,Θ,a)
f(800,Θ,a)
f(1000,Θ,a)
1.2
1
0.8
0.6
0.4
0.2
0
0.2
0.3
0.4
0.5
0.6
0.7
0.8
0.9
a
ASPERITY RATIO
100 m/s < V < 1000 m/s

Fig.18c

V := 1, 1.2.. 10

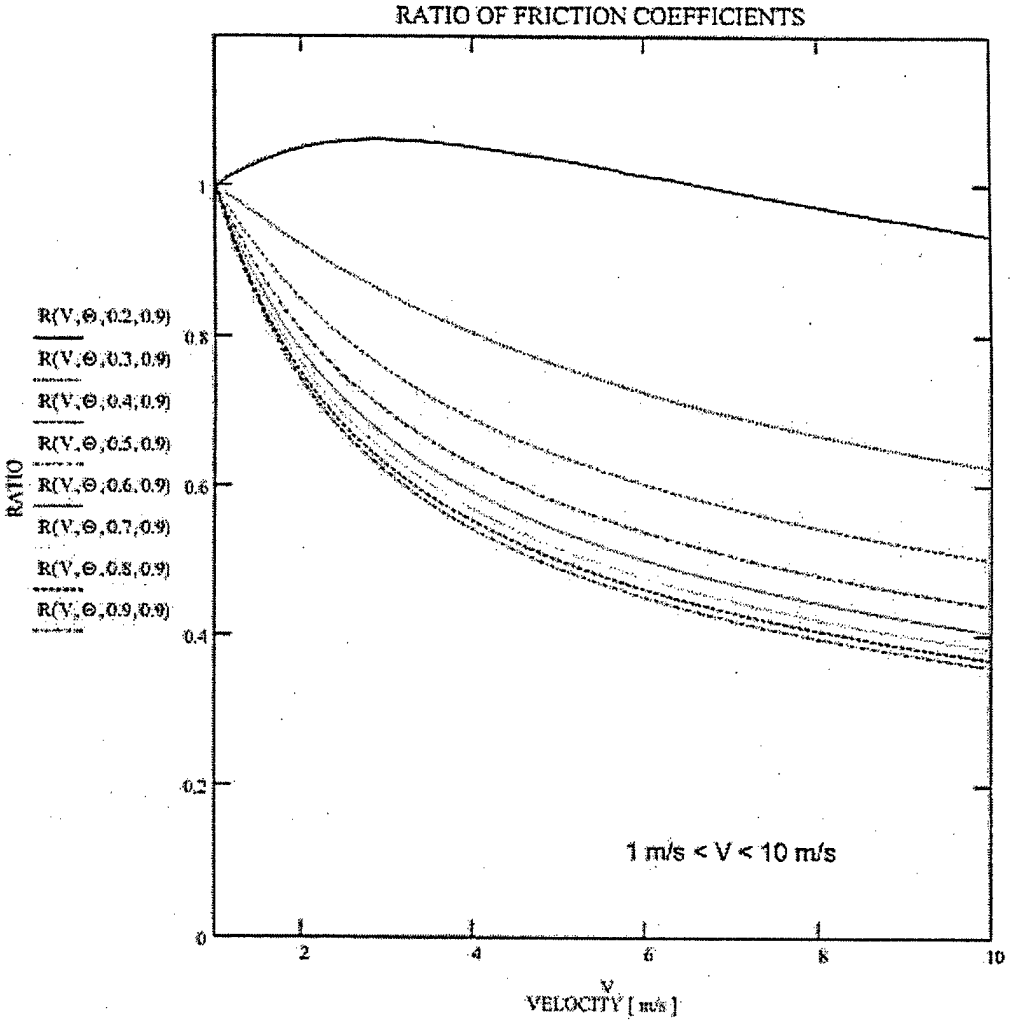

Fig.19a

V := 10, 12.. 100

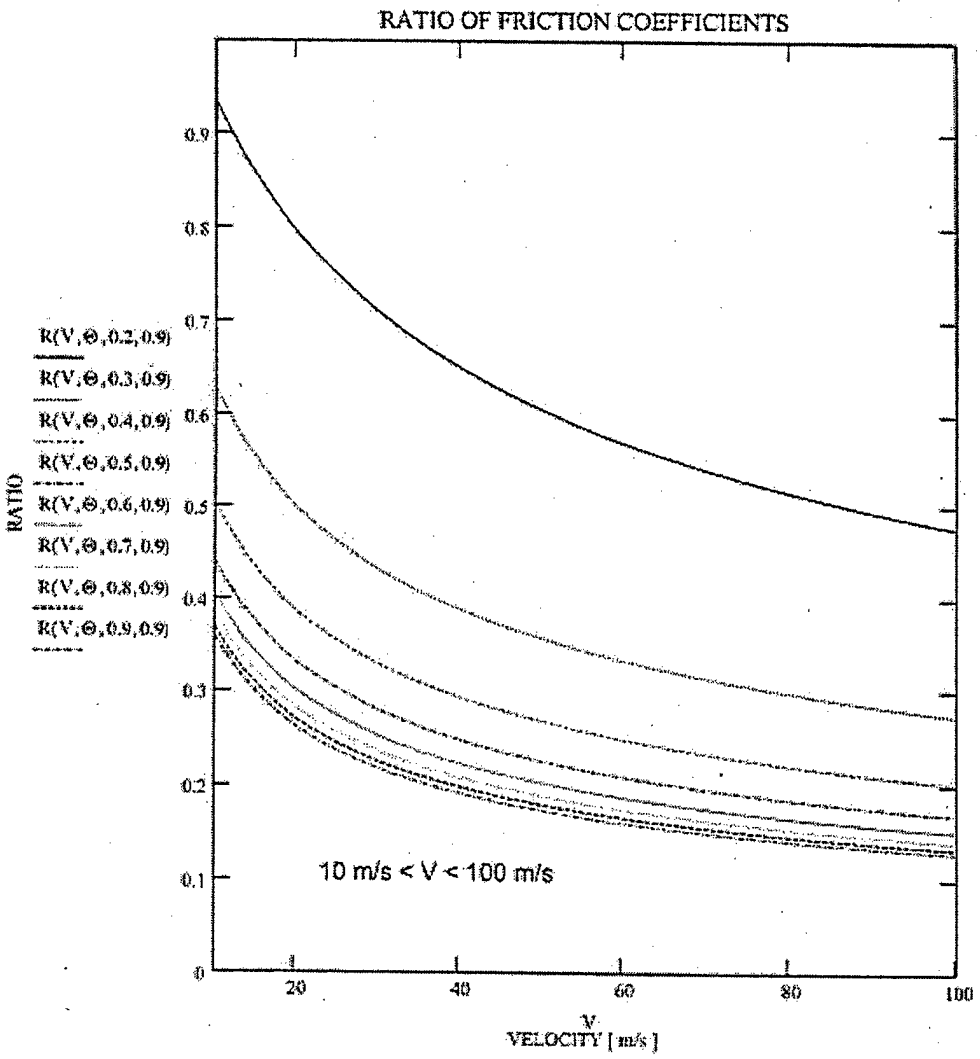

Fig.19b

$V := 100, 120 .. 1000$

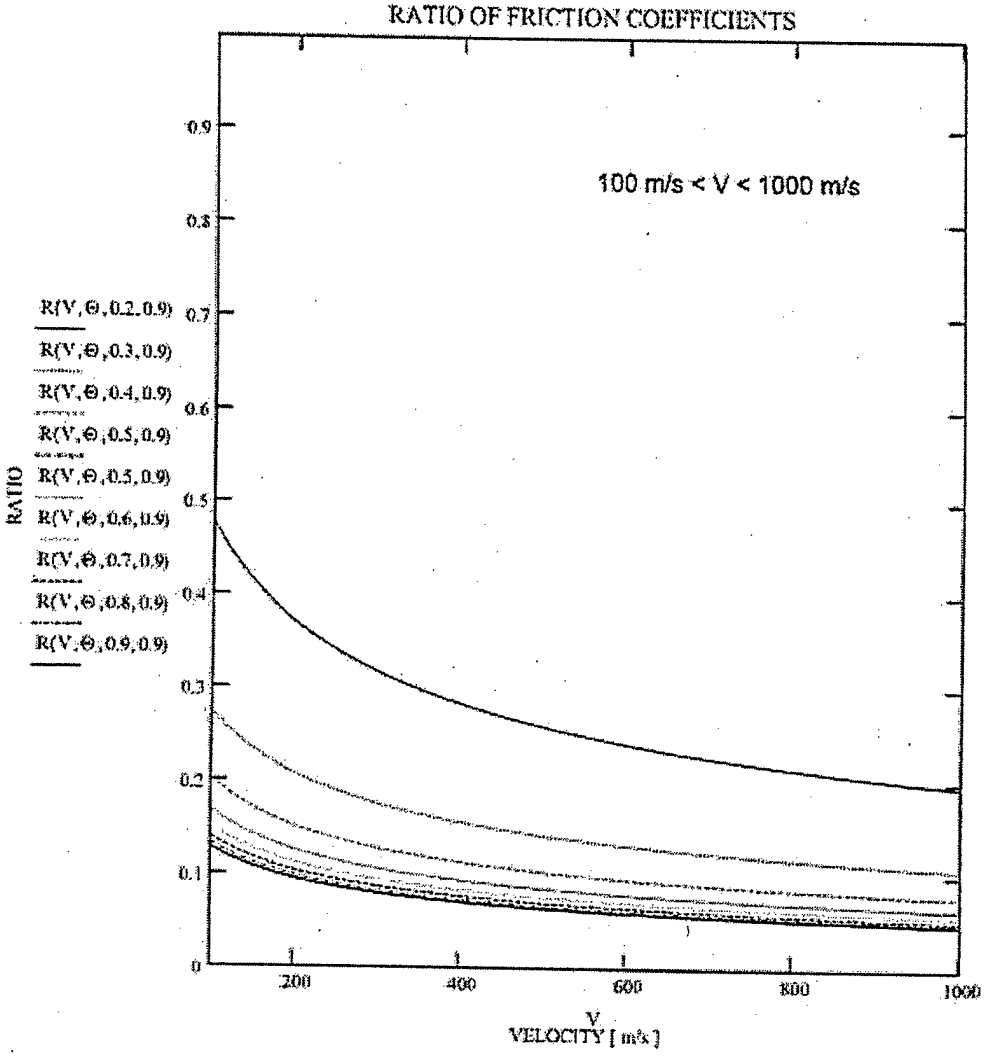

Fig.19c

$V := 1, 2 .. 1000$

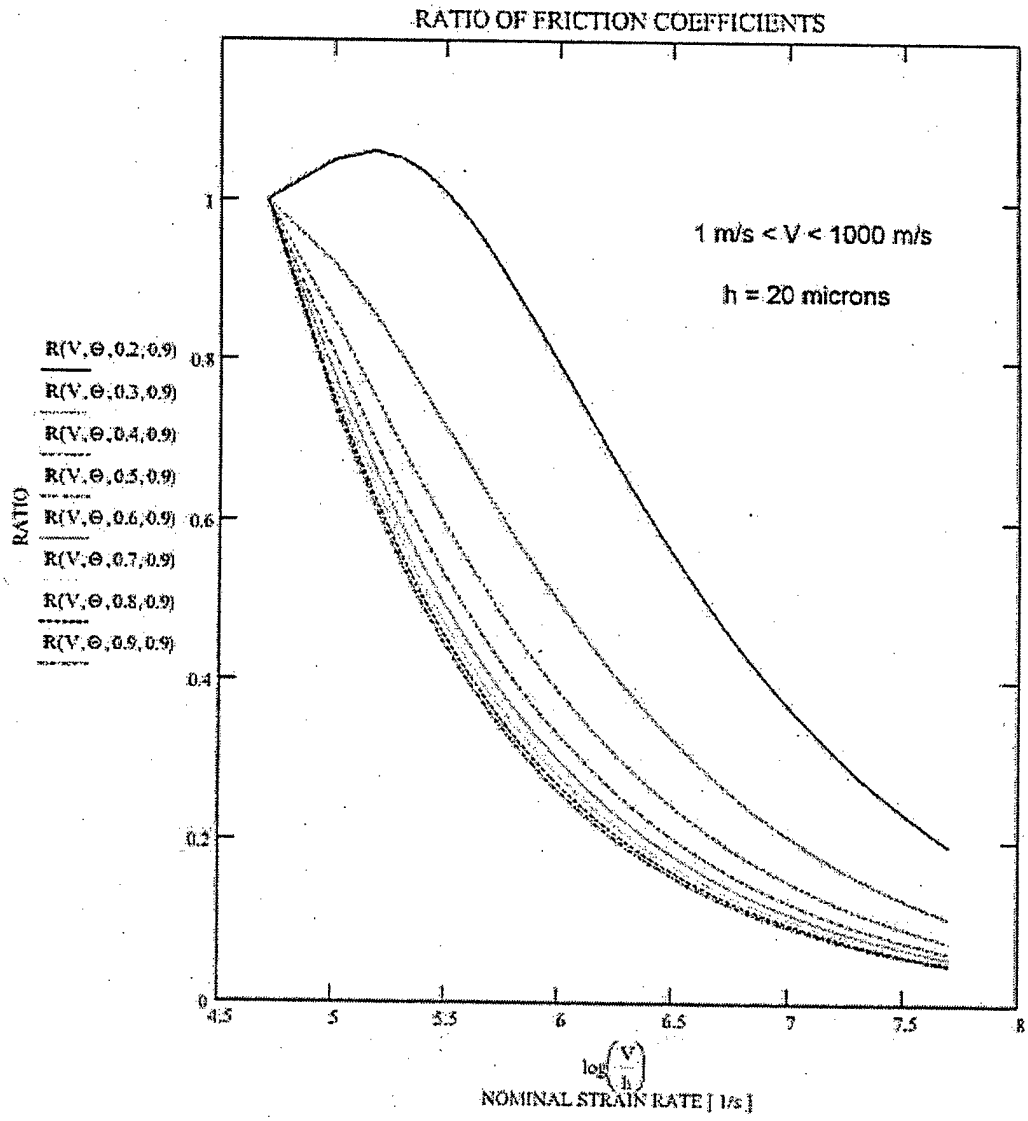

Fig.20

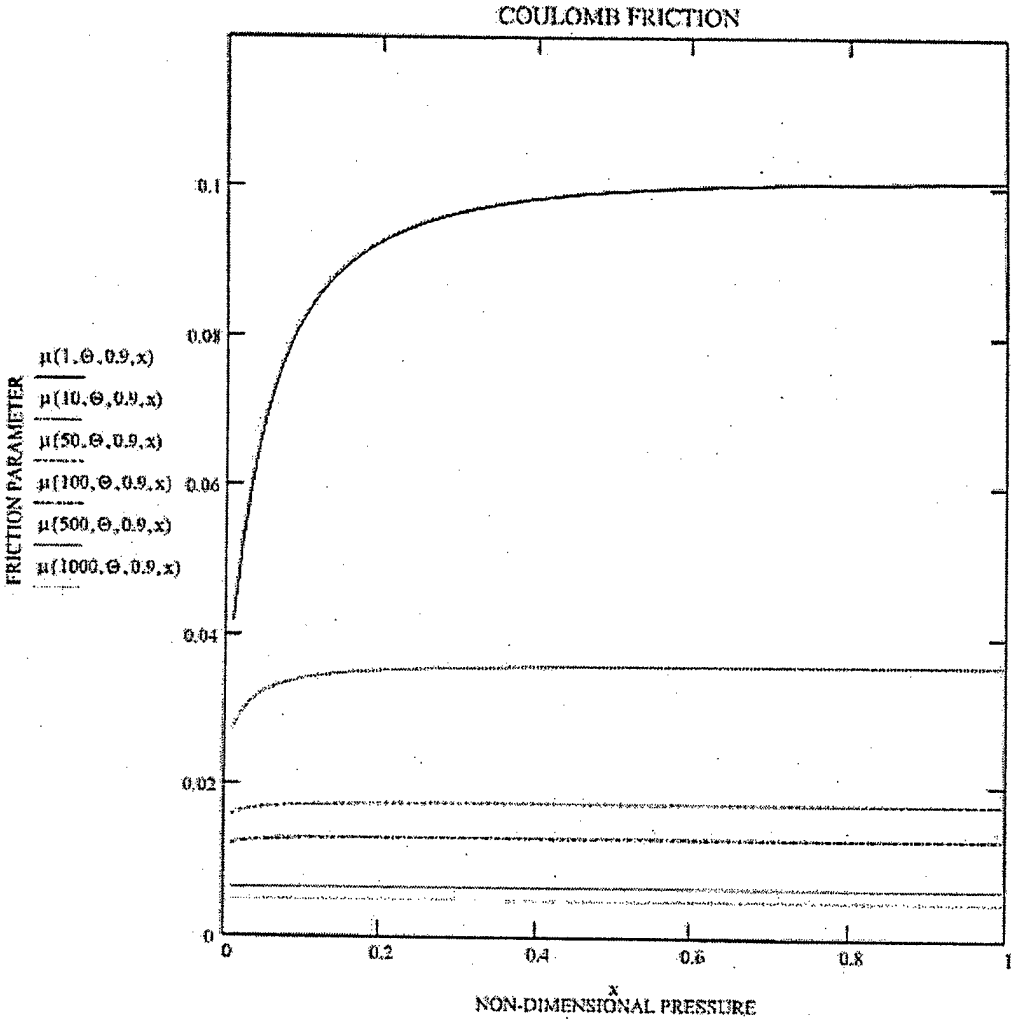
COULOMB FRICTION
FRICTION PARAMETER
μ(1,Θ,0.9,x)
μ(10,Θ,0.9,x)
μ(50,Θ,0.9,x)
μ(100,Θ,0.9,x)
μ(500,Θ,0.9,x)
μ(1000,Θ,0.9,x)
0.1
0.08
0.06
0.04
0.02
0
0
0.2
0.4
0.6
0.8
1
x
NON-DIMENSIONAL PRESSURE

Fig.21

V := 1, 1.2.. 10

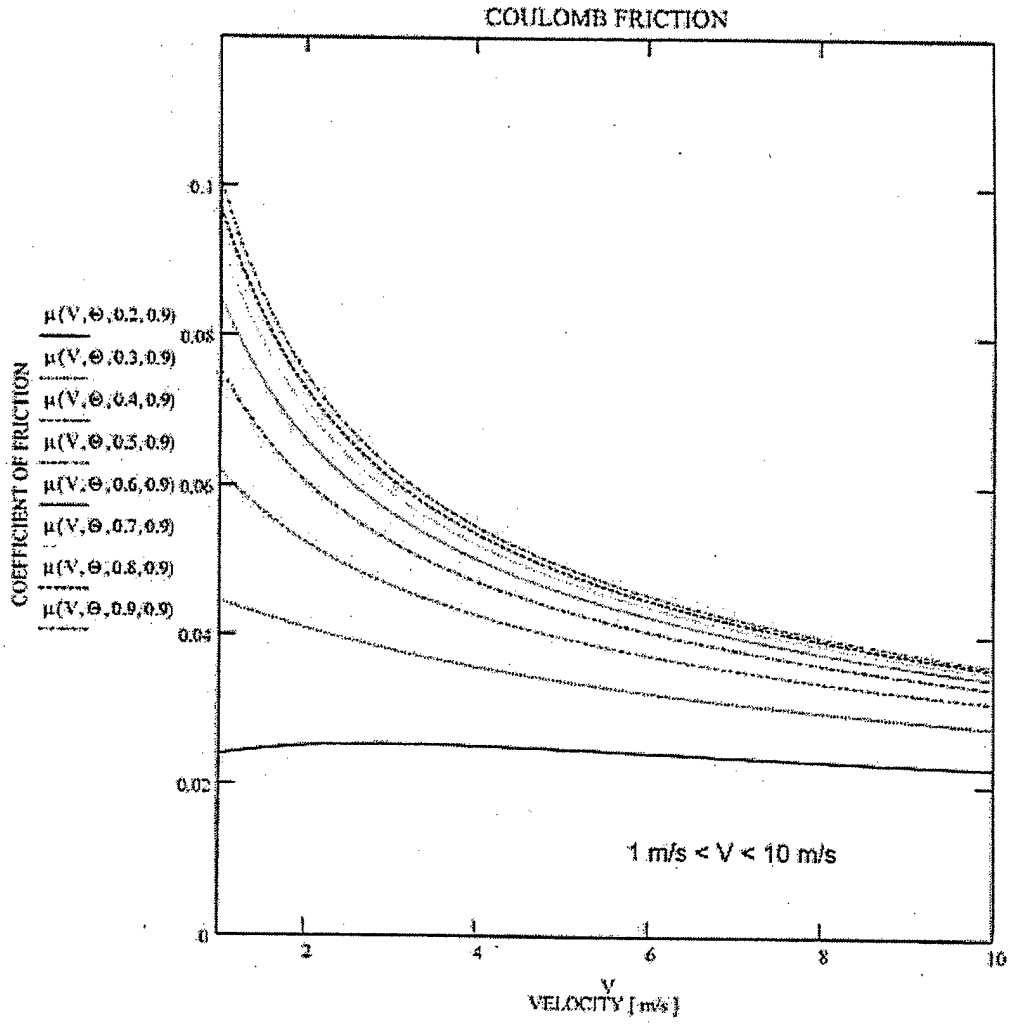

Fig.22a

$V := 10, 12 .. 100$

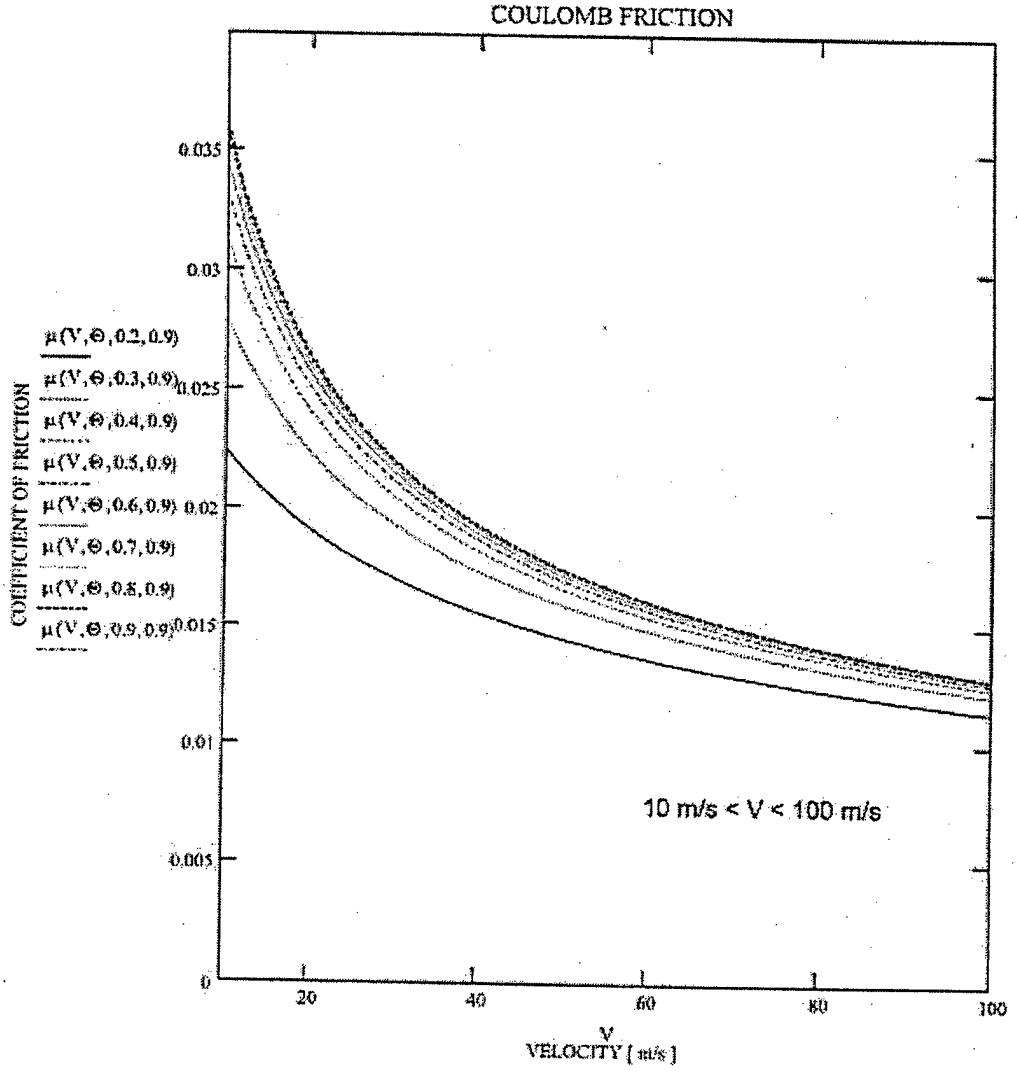

Fig.22b

V := 100, 120.. 1000

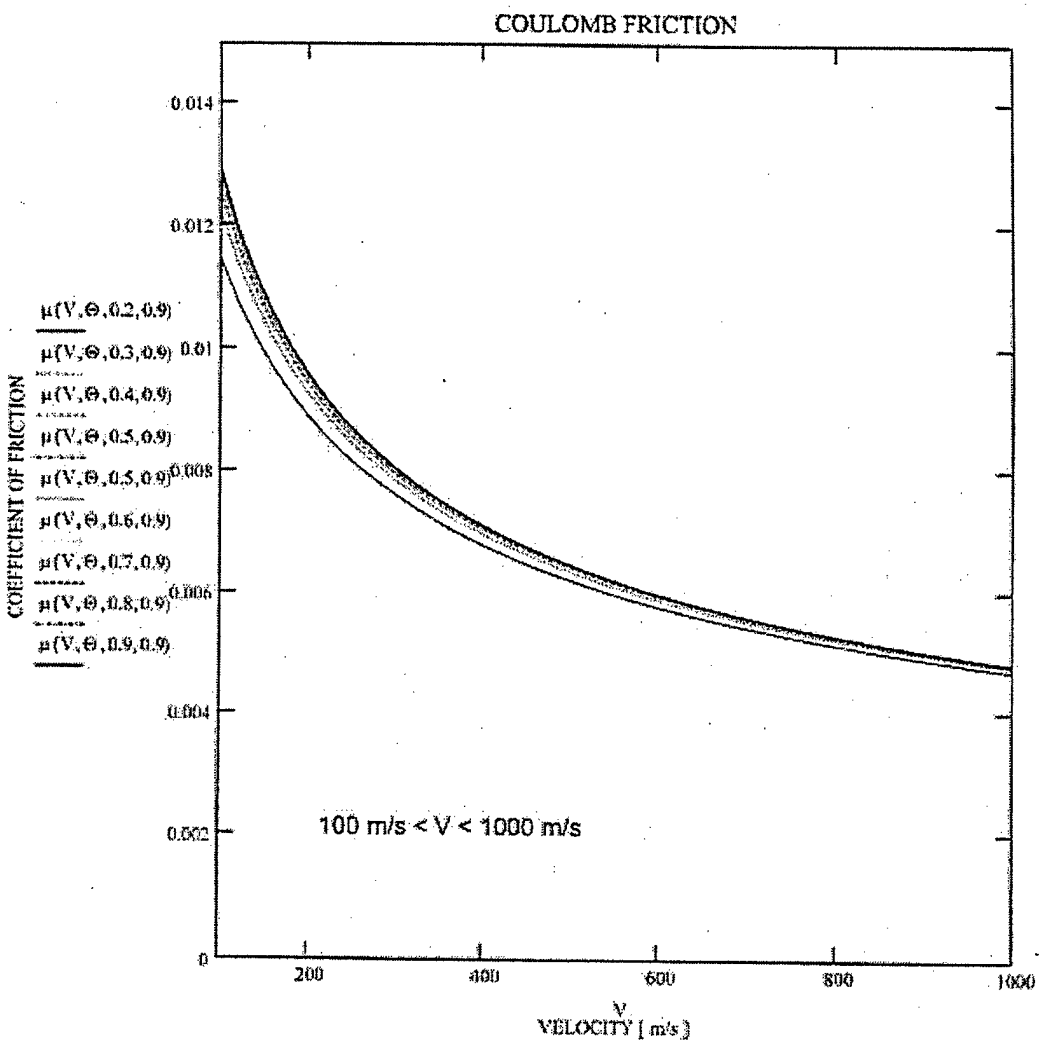

Fig.22c

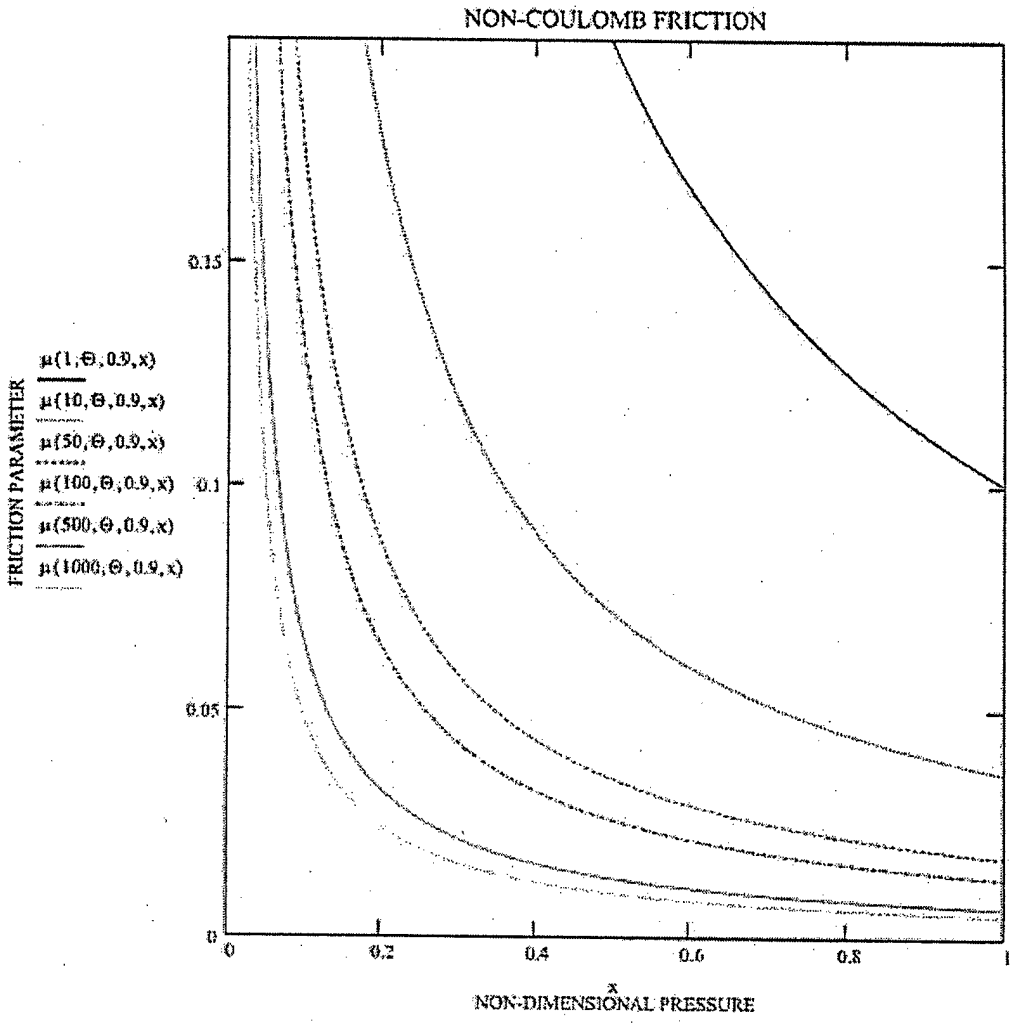
NON-COULOMB FRICTION
FRICTION PARAMETER
μ(1,Θ,0.9,x)
μ(10,Θ,0.9,x)
μ(50,Θ,0.9,x)
μ(100,Θ,0.9,x)
μ(500,Θ,0.9,x)
μ(1000,Θ,0.9,x)
0.15
0.1
0.05
0
0
0.2
0.4
0.6
0.8
1
x
NON-DIMENSIONAL PRESSURE

Fig.23

$V := 1, 1.2 .. 10$

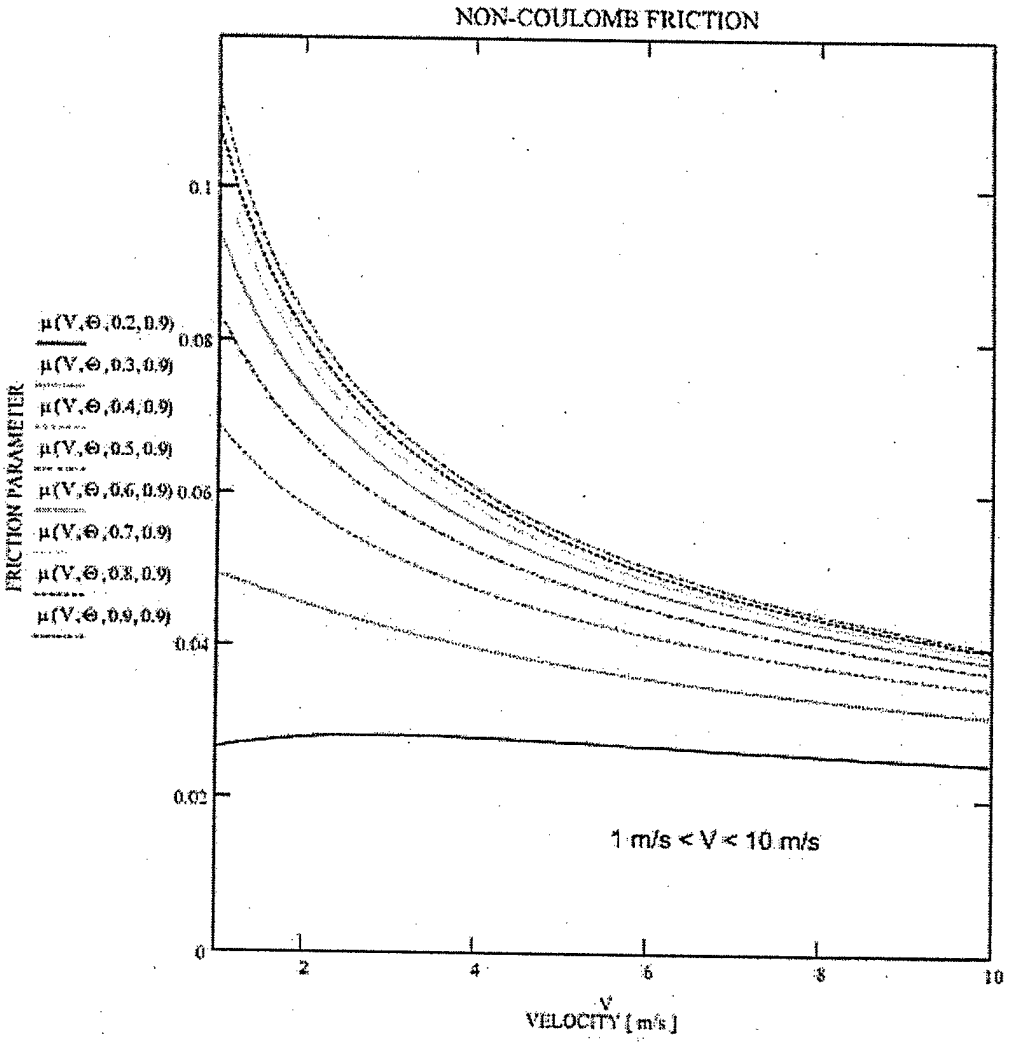

Fig.24a

V := 10, 15.. 100

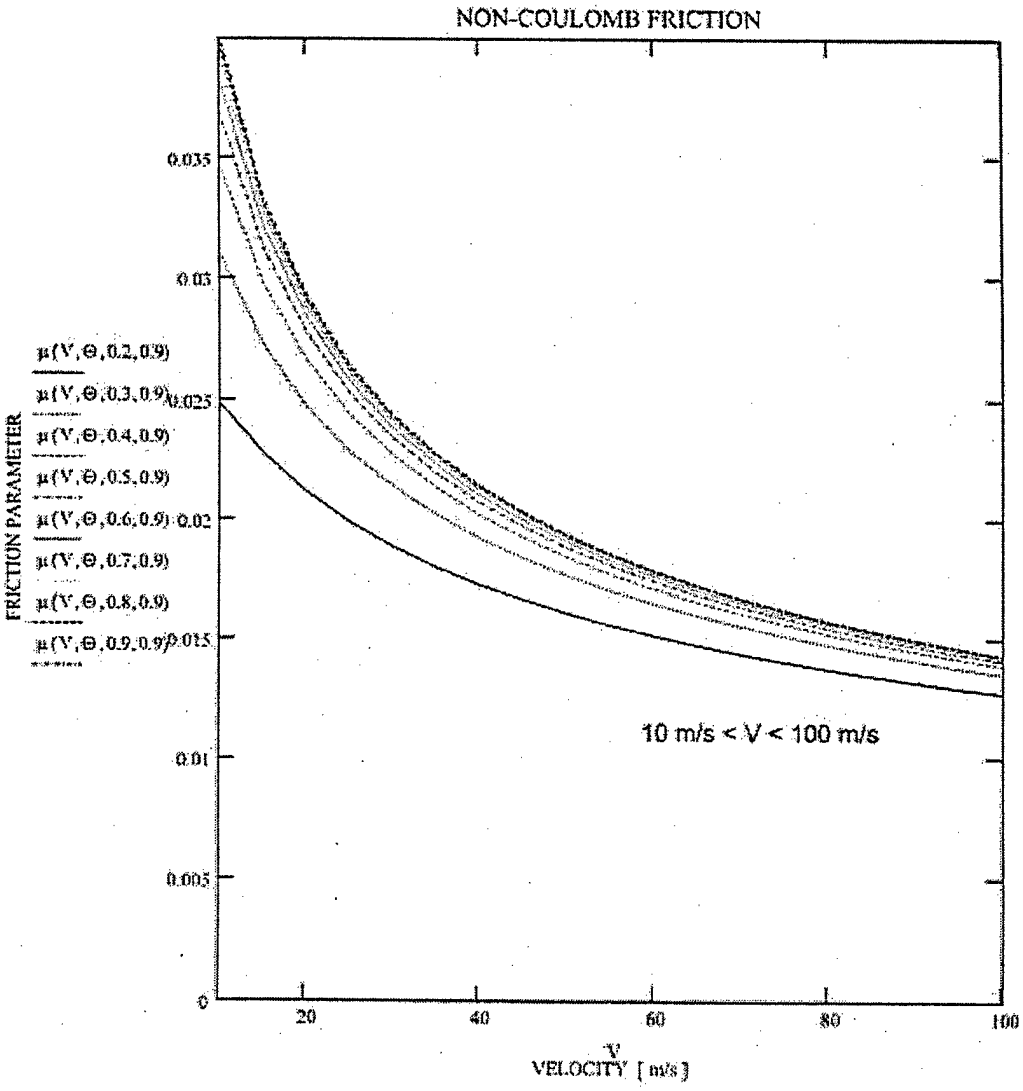

Fig.24b

$V := 100, 150 .. 1000$

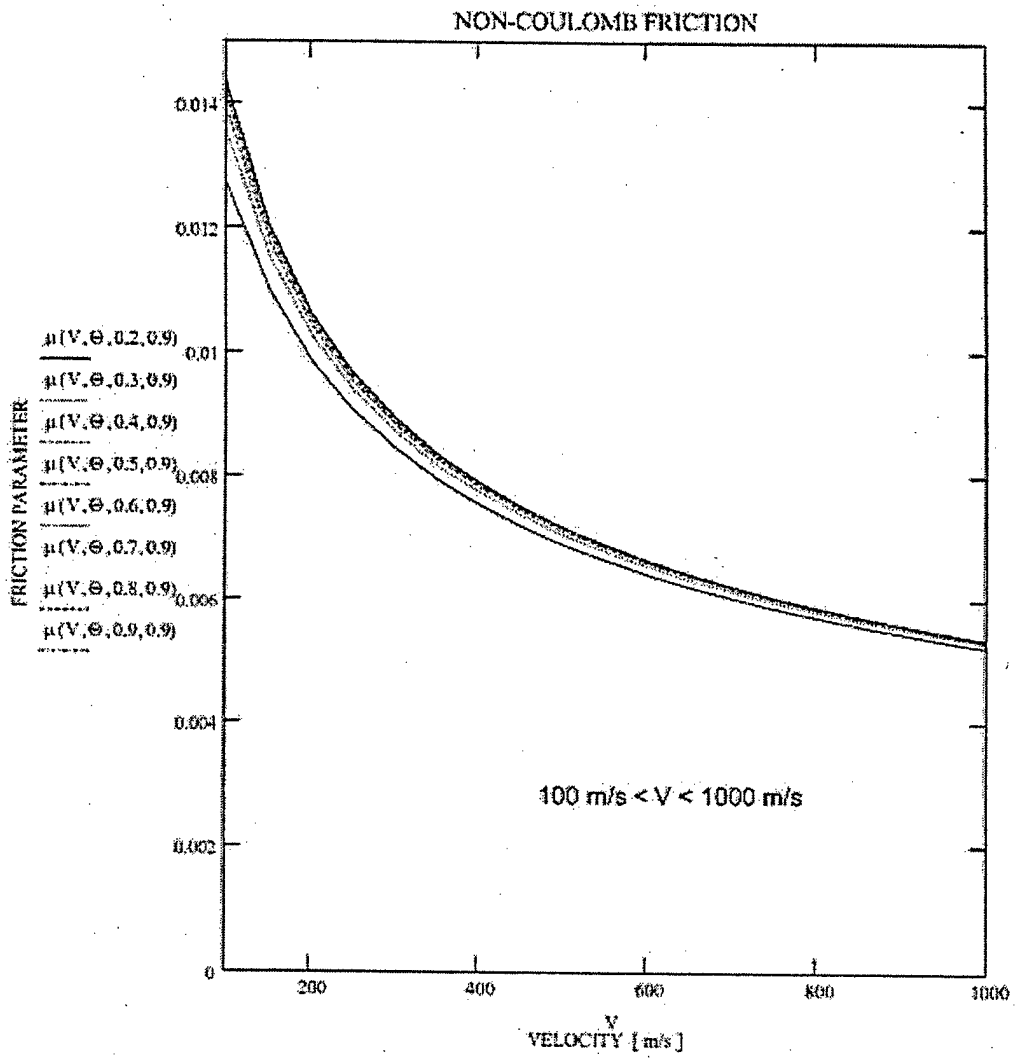

Fig.24c

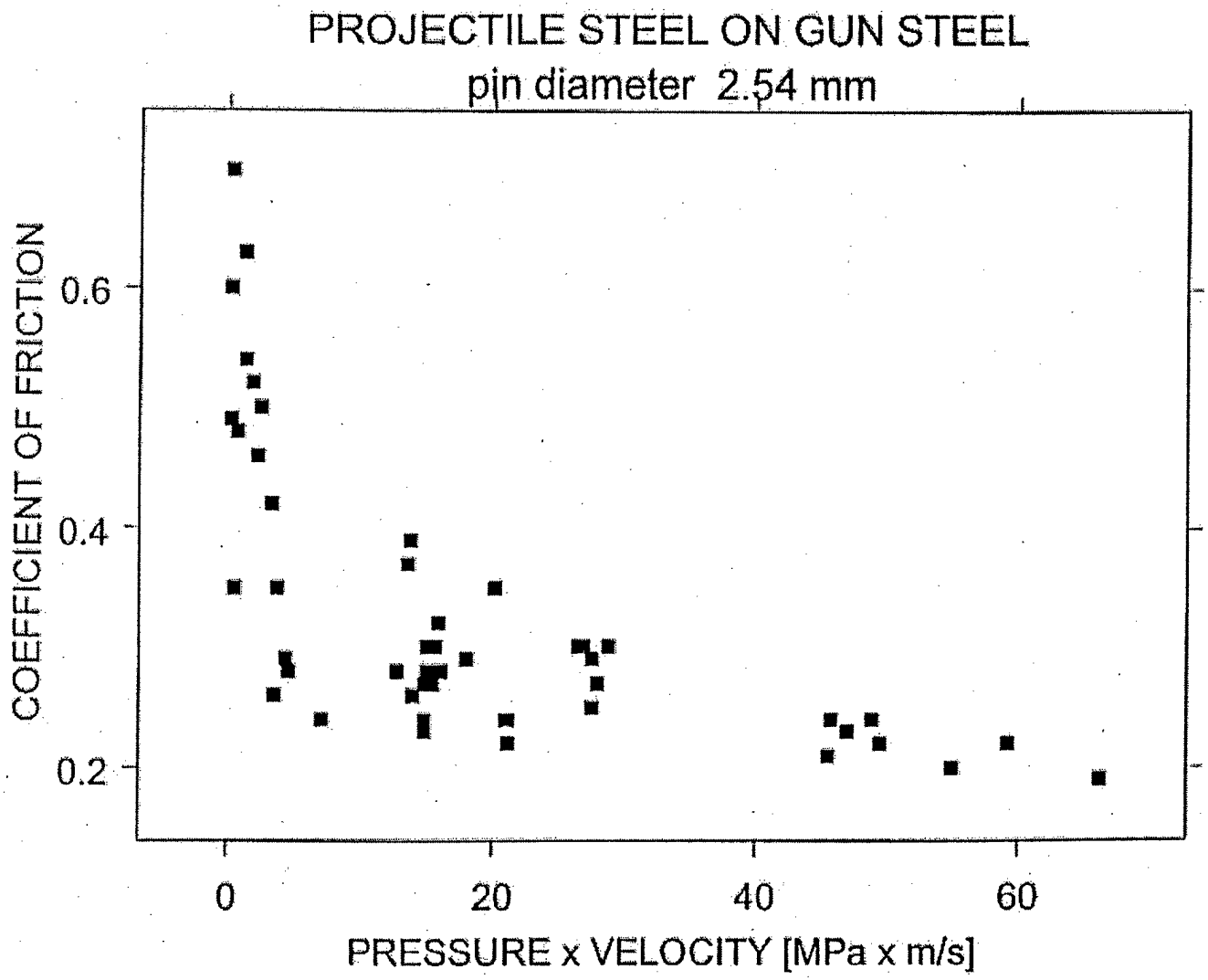
PROJECTILE STEEL ON GUN STEEL
pin diameter 2.54 mm
COEFFICIENT OF FRICTION
0.6
0.4
0.2
0
20
40
60
PRESSURE x VELOCITY [MPa x m/s]

Fig.25

DISTRIBUTION LIST
AFRL-MN-EG-TR-2001-7076

Defense Technical Information Center 8725 John J. Kingman Road, Ste 0944 Ft. Belvoir, VA 22060-6218	1 Copy

EGLIN AFB OFFICES:

AFRL/MN CA-N	1 Copy
AFRL/MNOC-1 (STINFO Office)	1 Copy
AFRL/MNAC	1 Copy
AFRL/MNMW	2 Copies

University of Florida Graduate Engineering and Research Center 1350 North Poquito Road Shalimar, Florida 32579-1163	1 Copy